AAAM 64th Annual Scientific Conference

October 12 - October 16, 2020

Short Communications

Tuesday, 10/13/2020
3:30 PM - 4:40 PM: Non-Standard Seating and Simulations

Tuesday, 10/13/2020, 4:00 PM - 04:10 PM EST
Finite Element Reconstruction of a Vehicle-to-Pedestrian Impact
Author: Casey Costa, ccosta@wakehealth.edu
Co-Authors: Jazmine Aira, jaira@wakehealth.edu, Bharath Koya, bkoya@wakehealth.edu, William Decker, wdecker@wakehealth.edu, Joel Sink, josink@wakehealth.edu, Shanna Withers, swithers@wakehealth.edu, Rukiya Beal, rabeal@wakehealth.edu, Sydney Schieffer, sschieff@wakehealth.edu, Scott Gayzik, sgayzik@wakehealth.edu,
Joel Stitzel, jstitzel@wakehealth.edu, Ashley Weaver, asweaver@wakehealth.edu

ABSTRACT
Objective: This study aims to reconstruct a real-world Crash Injury Research and Engineering Network vehicle-to-pedestrian impact to supplement the determination of pedestrian kinematics and injury causation.
Methods: A case involving a 46-year-old male pedestrian with a height of 163 cm and mass of 100 kg that was impacted by a 2019 Dodge Charger Pursuit police cruiser at an approximate velocity of 20.1 m/s was reconstructed. The case vehicle was represented by a rigid shell of a 2019 Dodge Charger vehicle exterior from an open-source database. The case pedestrian was represented by the Global Human Body Models Consortium (GHBMC) 50th percentile male simplified pedestrian human body model. The GHBMC model was isometrically scaled to a height of 163 cm and the external layer of flesh was morphed to a male reference geometry with the same age, height, and body mass index as the case pedestrian. The approximate location and position of the pedestrian at the time of impact was determined from case vehicle dashboard camera images and the pedestrian model was adjusted accordingly.
Results: Reconstruction kinematics aligned with proposed CIREN case kinematics. The GHBMC model predicted fractures of the left inferior ischiopubic ramus, superior pubic ramus, ilium, sacral ala, acetabulum, and right ilium.

Conclusions: Finite element reconstructions of real-world pedestrian impacts are useful for analyzing pedestrian kinematics and provide an effective tool for improving pedestrian impact injury analyses.

INTRODUCTION

Approximately 1.35 million people are killed in motor vehicle crashes (MVCs) annually worldwide, 22% of which are caused by vehicle-to-pedestrian impacts (VPIs) (WHO, 2018). Finite element (FE) human body models (HBMs) and generic vehicle models have been validated and implemented as useful tools for studying pedestrian kinematics and injuries in standardized settings (Klug et al., 2017, Decker et al., 2019). However, less work has been focused on real-world VPIs, which involve more variability (Lalwala et al., 2019). The Crash Injury Research and Engineering Network (CIREN) Pedestrian Pilot Study performs detailed investigations of real-world pedestrian impacts to develop a better understanding of pedestrian kinematics and injury causation. FE reconstructions of CIREN cases may be used to supplement these investigations. The objective of this study was to reconstruct a CIREN pedestrian impact and compare the reconstruction to the actual case to determine the utility of reconstructions to CIREN case reviews.

METHODS

Case Details. The case pedestrian was a 46-year-old male with a height of 163 cm and a mass of 100 kg. The case vehicle was a 2019 Dodge Charger Pursuit police cruiser traveling at a velocity of 20.1 m/s (45 miles/hr). The case pedestrian's left side was impacted by the left front corner of the vehicle and he sustained fractures of the left inferior ischiopubic ramus, superior pubic root, ilium, sacral ala, acetabulum, left ulna, left ribs 3-5 and right ribs 3-4. Proposed case kinematics involved left hip contact to the hood, followed by left elbow contact to the windshield and A-pillar, followed by thorax contact to the left side mirror. The CIREN Pedestrian Pilot Study uses AIS 2015 and multiple authors of this study, including the primary author, have experience coding injuries in CIREN using AIS.

Reconstruction Methodology. The case vehicle was represented by a rigid shell of a 2019 Dodge Charger vehicle exterior from an open-source database. The case pedestrian was represented by the Global Human Body Models Consortium (GHBMC) 50th percentile male simplified pedestrian HBM (Untaroiu et al., 2018). The pedestrian model was isometrically scaled to a height of 163 cm and the external layer of flesh was morphed to a standing male reference geometry with the same age, height, and body mass index as the case pedestrian, which was obtained from population-based models provided by humanshape.org. The approximate location, orientation, and leg position of the pedestrian at the time of impact was determined from case vehicle dashboard camera images (Figure 1) and vehicle deformation. The GHBMC model was given an arbitrary initial forward velocity of 3.4 m/s to simulate running of the case pedestrian. The vehicle model was assigned a constant velocity of 20.1 m/s (45 miles/hr).

RESULTS

Reconstruction kinematics aligned closely with the proposed kinematic scenario from the CIREN case review (Figure 2). The left hip of the GHBMC model contacted the hood in the same location as the case vehicle hood deformation. The GHBMC model left shoulder, thorax, and arm contacted the left side mirror 86 ms after hip contact, but in an anatomical location superior to the case pedestrian. The left elbow did not contact the windshield or A-pillar, but

came within 11 cm of them. The GHBMC model predicted fractures of the left inferior ischiopubic ramus, left superior pubic ramus, left ilium, left sacral ala, left acetabulum, and right ilium (Figure 3), during hip-to-hood impact.

DISCUSSION

The reconstruction overpredicted the number of pelvis fractures compared to the case pedestrian, but accurately predicted what specific regions of the pelvis were fractured for 4 of the 5 case fractures (inferior pubic ramus, ilium, sacral ala, acetabulum). The current reconstruction displays injury-prediction capabilities that may be better than expected for real-world crashes. Lalwala et al (2019) reconstructed 3 real-world crashes using the Total Human Model for Safety (THUMS) HBM and correctly predicted fractures in 2 of them. Discrepancies between case pedestrian and reconstruction kinematics and injuries can be explained by multiple limitations. The vehicle model was made rigid, but real-world vehicles are able to deform. Additionally, it is common for pedestrians to actively attempt to avoid impact or brace themselves by raising their arms upon the realization of an impending impact (Soni et al., 2013). This was not included in the reconstruction. If the pedestrian attempted to avoid the vehicle to mitigate the impact or raise his arms to brace himself, it may explain the discrepancies in pelvis fractures and elbow contact. Lack of variations regarding pedestrian posture, running speed, and active response to account for uncertainties are also limitations and will be addressed in future studies by conducting multiple simulations while adjusting each variable. Lastly, the methodologies for adjusting the GHBMC model (i.e, isometric scaling) may result in unrealistic morphological dimensions and subject-specific morphing using computed tomography will be explored in future reconstructions. To conclude, a CIREN pedestrian impact was reconstructed using a partially-morphed simplified GHBMC 50th percentile male HBM and a 2019 Dodge Charger rigid shell. Reconstruction kinematics and pelvis fractures closely aligned with the CIREN case, indicating that FE reconstructions may be useful supplements to CIREN case reviews, but additional reconstructions are required to establish their utility.

ACKNOWLEDGEMENTS

The authors would like to thank the National Highway Traffic Safety Administration who provided funding under the Crash Injury Research and Engineering Network Pedestrian Pilot study (DTNH2217D00070). Dr. Joel Stitzel and Dr. Scott Gayzik are members of Elemance LLC, which licenses and distributes the GHBMC human body model.

REFERENCES

Decker, W., Koya, B., Pak, W., Untaroiu, C.D. and Gayzik, F.S. Evaluation of finite element human body models for use in a standardized protocol for pedestrian safety assessment. Traffic Inj Prev. 2019. 20(sup2): S32-S36.

Klug, C., Feist, F., Raffler, M., Sinz, W., Petit, P., Ellway, J. and van Ratingen, M. Development of a Procedure to Compare Kinematics of Human Body Models for Pedestrian Simulations. International Research Council on Biomechanics of Injury Conference 2017. 2017. 508-530.

Lalwala, M., Chawla, A., Thomas, P. and Mukherjee, S. Finite element reconstruction of real-world pedestrian accidents using THUMS pedestrian model. International Journal of Crashworthiness. 2019.

Soni, A., Robert, T., Rongieras, F. and Beillas, P. Observations on pedestrian pre-crash reactions during simulated accidents. Stapp Car Crash J. 2013. 57: 157-183.

Untaroiu, C.D., Pak, W., Meng, Y., Schap, J., Koya, B. and Gayzik, F.S. A Finite Element Model of a Midsize Male for Simulating Pedestrian Accidents. J Biomech Eng. 2018. 140(1).
WHO (2018). Global Status Report on Road Safety. 2018;

FIGURES

Figure 1. Dashboard camera footage of case pedestrian (*yellow arrow*) prior to impact.

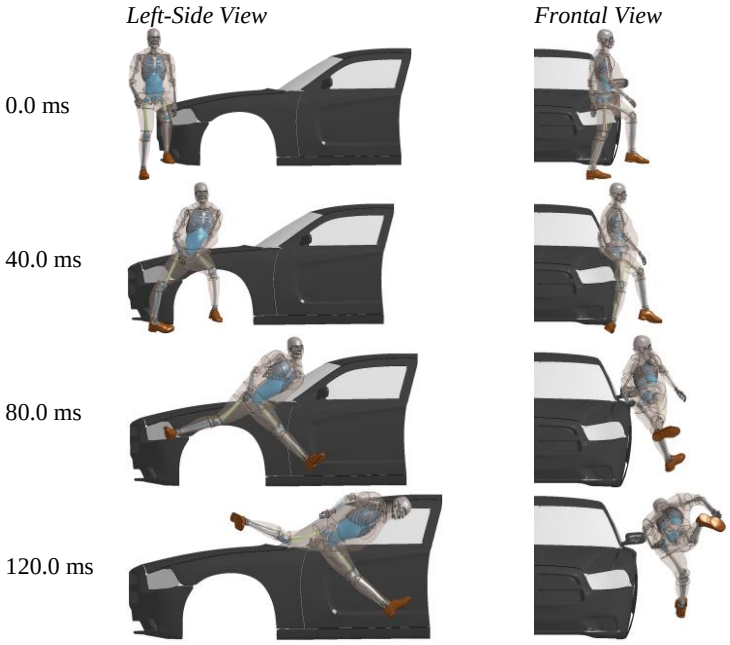

Figure 2. Pedestrian kinematics from the left-side and front views.

Figure 3. Comparison of pelvis injuries between case pedestrian (left and center) and GHBMC model (right). Red arrows indicate locations of fracture

Wednesday, October 14th, 2020
11:30 AM - 1:25 PM: Vulnerable Population

Wednesday, October 14th, 2020, 12:00 PM - 12:10 PM EST
Selected Characteristics and Injury Patterns by Age Group Among Pedestrians Treated in North Carolina Emergency Departments
Author: Katherine J. Harmon, harmon@hsrc.unc.edu
Co-Authors: Kari A. Hancock, hancock@hsrc.unc.edu, Anna E. Waller, anna_waller@med.unc.edu, Laura S. Sandt, sandt@hsrc.unc.edu

ABSTRACT
Objective: To describe pedestrian demographic characteristics, crash characteristics, selected health outcomes, and injury patterns by age using linked North Carolina (NC) crash-emergency department (ED) visit data for the period October 1, 2010 – September 30, 2015.
Methods: This was a descriptive epidemiologic study. To examine both crash and health outcomes, NC pedestrian crash records were linked to statewide NC ED visit records using hierarchical deterministic methods. Pearson chi-square tests were used to compare the frequencies of pedestrians treated in NC EDs by sex, race/ethnicity, crash location, rurality, estimated driver speed at impact, ambient light, hospitalization/death, location of injury, and nature of injury, stratified by the following age groups: 0-14, 15-24, 25-64, and ≥65 years.
Results: Most pedestrians treated in NC EDs were male (57.5%), except among adults ≥65 years-old (47.5%). Over half of all injured pedestrians 0-14 (52.6%) and 15-24 (50.5%) years were Black/African-American, while injured pedestrians ≥65 years were 70.8% White. Among pedestrians 25-64 years, no single racial/ethnic group was the majority. While most pedestrians were injured on trafficways (71.7%) and at speeds ≤35 miles per hour (MPH) (80.1%), adults ≥65 years were less likely to be involved in on-trafficway crashes (51.0%) and pedestrians 15-24 years were more likely to be involved in >35 MPH crashes (22.9%), as compared to other age groups. Most pedestrians were injured under daylight conditions (56.9%).

Regarding selected health outcomes, the highest frequency of hospitalization/death was for pedestrians ≥65 years (26.3%), compared to those 0-14 years (18.8%) and 15-64 years (12.4%). In terms of location of injury, 0-14-year-olds had the highest proportion of head injuries (39.5%), while adults ≥65 years-of-age had the highest proportion of spinal column/vertebral column (12.6%) and upper extremity injuries (33.2%). For nature of injury, 0-14-year-olds had the highest proportion of traumatic brain injuries (11.4%) and superficial wounds and contusions (62.8%). Adults ≥65 years had the highest proportion of open wounds/amputations and fractures (16.1%). Adults 25-64 years had the highest proportion of strains/sprains/dislocations (18.7%).
Conclusions: There were considerable differences in demographic characteristics, crash characteristics, frequency of hospitalization/death, and injury patterns by age group. It is important to design streets and implement transportation policies and programs that improve safety for all pedestrians.

INTRODUCTION
From 2009 to 2018, the number of United States (US) pedestrian fatalities increased by 53% (Retting 2020). The mechanism for this rise is complex and multifactorial, with changes in vehicle miles traveled, vehicle fleet composition, driver/pedestrian distraction and impairment, support for pedestrian safety and infrastructure, and other factors each playing a contributing role

(Sandt et al. 2020). An important consideration is the changing demographic composition of the US population. From 2016 to 2060, the US population of adults ≥65 will nearly double, from 49 to 98 million individuals, an increase from 15% to 23% of the population (Vespa et al. 2020). Older adults may be at an increased risk of being struck by motor vehicles because of age-related physical, sensory, and cognitive declines (Chakravarthy et al. 2007). In addition, compared to younger adult pedestrians, older pedestrians are more likely to be hospitalized and die from their injuries (Demetriades et al. 2004). Understanding differences in patient and crash characteristics and injury patterns is essential for the development of targeted pedestrian safety policies and programs. The objective of this study is to describe pedestrian demographic and crash characteristics, selected health outcomes, and injury patterns by age using linked North Carolina (NC) crash-emergency department (ED) visit data for the period October 1, 2010 – September 30, 2015.

METHODS

This study was approved by the University of North Carolina (UNC) at Chapel Hill Institutional Review Board.

Data Sources and Linkage

North Carolina (NC) crash and emergency department (ED) visit data were linked and analyzed to describe collision circumstances and health outcomes of pedestrians involved in police-reported motor vehicle crashes.

NC pedestrian crash data The UNC Highway Safety Research Center (UNC HSRC) provided pedestrian crash data. UNC HSRC maintains an electronic database of all NC police-reported collisions between pedestrians and motor vehicles. This database includes elements documented in the police crash report form and information abstracted from the crash diagram and narrative (Thomas et al. 2018).

NC ED visit data The NC Division of Public Health (NC DPH) provided ED visit data. NC DPH captures information on all patients treated at 24/7 acute-care hospital-affiliated civilian NC EDs, as part of NC DETECT, NC's legislatively mandated statewide syndromic surveillance system (CCHI 2020). For inclusion in the study, the pedestrian ED visit record had to contain an International Classification of Disease, 9th Revision, Clinical Modification (ICD-9-CM) injury diagnosis code (800-999) or external cause of injury code (E-code) (NCHS, CDC 2015). To avoid one-to-many linkages, patient transfers to other healthcare institutions were excluded.

Linkage NC pedestrian crash (N=14,264) and ED visit (N=4,181,226) data were linked for the period October 1, 2010 – September 30, 2015. This five-year period was selected to avoid the transition from ICD-9-CM to ICD-10-CM, a period which resulted in significant changes in healthcare data (Slavova et al. 2018). Data were linked using a hierarchical deterministic method. An overview of methods is described elsewhere (Harmon et al. 2019). A total of 6,919 pedestrian crash records were linked to ED visit records (48.5%).

Measures

Demographic variables Demographic variables selected for analysis were age, categorized into groups corresponding to children (0-14), youth and young adults (15-24), working-age adults (25-64), and older adults (≥65 years of age); sex; and race/ethnicity (White, Black/African-American, other race/ethnicity). All demographic variables, except race/ethnicity, were selected from the ED visit data. NC ED visit data did not capture race/ethnicity during 2010-2015, so this information was abstracted from the crash data.

Crash variables Crash variables selected for analysis were crash location (public trafficway versus non-trafficway [e.g. parking lots]), rurality (urban versus rural), ambient light (light, dawn/dusk, dark), and estimated driver speed at impact. Estimated driver speed at impact was categorized into ≤35 miles per hour (MPH) and >35 MPH, based on pedestrian risk fatality curves (DC Richards Transport Research Laboratory 2010).

Emergency department variables Emergency department visit variables selected for analysis were nature of injury and injury location. ICD-9-CM injury diagnoses were categorized using the Barell Injury Diagnosis Matrix (Barell et al. 2002). For pedestrians with more than one injury, each injury was categorized separately. ICD-9-CM injury diagnosis codes were not mapped to Abbreviated Injury Scale (AIS) scores due to the lack of specificity of the available diagnosis codes.

A composite hospital admission/death variable was created from the crash and ED visit data. A patient was classified as admitted/died if they had crash injury severity score of "K-killed" or had an ED visit discharge disposition of "Admitted to the hospital" or "Died."

Analyses

This study examined pedestrian crash and ED visit characteristics, stratified by patient age group. For statistical comparisons, this study used Pearson chi-square test. Significance was assessed at an alpha value of 0.05. Statistical analyses for this study were performed using SAS® version 9.4 (SAS Institute, Cary, NC).

RESULTS

Demographic patterns differed by age group for pedestrians treated in NC EDs following police-reported motor vehicle crashes (Table 1). Most pedestrians were male (57.5%), except among older adults, in which 52.5% of all patients treated were female. There were also differences by race/ethnicity, with over half of all injured pedestrians 0-14 (52.6%) and 15-24 (50.5%) years being Black/African-American.

Most pedestrians were injured in urban crashes (73.4%) on the public trafficway (71.7%). However, adults ≥65 years were less likely to be involved in on-trafficway crashes (51.0%) (Table 1). Older adult pedestrians were also more likely to be involved in crashes with impact speeds of ≤35 MPH (89.8%). There were also age group differences by ambient light. For example, 45.8% of injured pedestrians 15-24 years of age were injured under dark conditions, while only 17.8% of older adults were injured under dark conditions.

[Insert Table 1]

There were also significant differences in health outcomes and injury patterns across the lifespan. Hospital admission/death differed by age group (P= <.001). Older adults (26.3%) and children (18.8%) were more likely to be admitted or die from their injuries compared to pedestrians 15-24 (13.6%) and 25-64 years of age (16.0%). Tables 2 and 3 display the location and nature of injury, respectively. Children were more likely to sustain injuries to the head (39.5%), traumatic brain injuries (TBIs) (11.4%), and superficial wounds/contusions (62.8%) than other age groups. For several injury types, there was an observed increase in frequency with age. For example, the proportion of patients diagnosed with injuries to the spinal column (SC)/vertebral column (VC) and upper extremities increased with age (Table 2). The frequency of fracture diagnoses also increased with age, with older adults 1.5 times and 1.3 times more likely to be diagnosed with a fracture as compared to pedestrians 15-24 and 25-64 years, respectively (Table 3). Other injury diagnoses, such as open wounds/amputations, displayed a

"U-shaped" pattern, with children (14.7%) and older adults (16.1%) having greater frequencies of these potentially serious and debilitating injuries.
[Insert Table 2]
[Insert Table 3]

DISCUSSION

There are noteworthy differences across the lifespan relating to crashes characteristics, health outcomes, and injury patterns among pedestrians receiving treatment in EDs after involvement in police-reported motor vehicle collisions. While children and older adults were less likely to be injured in on-trafficway, higher speed crashes, these age groups were more likely to be hospitalized or die and were more likely to be diagnosed with injuries associated with prolonged disability and increased risk of complications, such as TBIs and open wounds/amputations. Of concern is the relatively high frequency of fractures among older pedestrians. While fractures are rarely a cause of mortality among younger adults, a study of major orthopedic trauma among adults $\geq$65 years found that 6.8% succumbed to their injuries within 30 days, versus 2.5% among adults <64 years (Herron et al. 2017).

As individuals are increasingly encouraged to walk as a form of healthy, low-impact physical activity, it is important to consider the increased risk of injury, especially among higher-risk populations such as children and older adults (Brewer et al. 2014; Morris and Hardman 1997). It is important to incorporate safety and universal design principles into the development of trafficways and adjacent public spaces, accommodating all road users to the greatest extent possible (Lid 2013). Design principles to safely accommodate older and younger road users include managing vehicle speeds and volume, designing safe and convenient crossings for pedestrians with slower walking speeds, providing adequate lighting and sight distances, and other approaches (Brewer et al. 2014; Dumbaugh et al. 2019).

This study had several limitations. Most notably, it has a "survivor bias" in that only pedestrians who survived their injuries long enough to be admitted to the ED were included in the study. Also, the linked crash-ED visit data only included pedestrians injured in collisions reported to the police, underreporting the total number of pedestrian crashes. Finally, this study involved secondary uses of both crash and ED visit data. While population-based secondary data sources have advantages in terms of cost and representation, there may be disadvantages related to data quality.

In conclusion, this study highlights key differences in pedestrian crash characteristics and injury patterns by age, with implications for future research, program, and policy development.

ACKNOWLEDGEMENTS

NC Division of Public Health Data Attribution and Disclaimer

NC DETECT is a statewide public health syndromic surveillance system, funded by the NC DPH Federal Public Health Emergency Preparedness Grant and managed through collaboration between NC DPH and UNC-CH Department of Emergency Medicine's CCHI. The NC DETECT Data Oversight Committee does not take responsibility for the scientific validity or accuracy of methodology, results, statistical analyses, or conclusions presented.

Funding

This study received support from the Collaborative Sciences Center for Road Safety, www.roadsafety.unc.edu, a United States Department of Transportation National University Transportation Center promoting safety.

REFERENCES

Barell V, Aharonson-Daniel L, Fingerhut LA, Mackenzie EJ, Ziv A, Boyko V, Abargel A, Avitzour M, Heruti R. An introduction to the Barell body region by nature of injury diagnosis matrix. *Inj Prev*. 2002;8(2):91–96.

Brewer M, Murillo D, Pate A. *Handbook for Designing Roadways for the Aging Population*. Washington, DC: FHWA; 2014.

CCHI. NC DETECT. 2020. Available at: https://ncdetect.org/. Accessed May 21, 2020.

Chakravarthy B, Lotfipour S, Vaca FE. Pedestrian injuries: emergency care considerations. *Cal. J. Emerg. Med.* 2007;8(1):15–21.

DC Richards Transport Research Laboratory. *Relationship between Speed and Risk of Fatal Injury: Pedestrians and Car Occupants*. London, UK: DOT: London; 2010.

Demetriades D, Murray J, Martin M, Velmahos G, Salim A, Alo K, Rhee P. Pedestrians injured by automobiles: relationship of age to injury type and severity. *J. Am. Coll. Surg.* 2004;199(3):382–387.

Dumbaugh E, Merlin L, Signor K, Kumfer W, LaJeunesse S, Carter D. *Implementing Safe Systems in the United States: Guiding Principles and Lessons from International Practice.* Chapel Hill: CSCRS; 2019.

Harmon KJ, Peticolas K, Waller AE. *Police Crash Report Data & NC DETECT Emergency Department Visit Data*. Chapel Hill, NC: CCHI, UNC SOM; 2019. Available at: http://cchi.web.unc.edu/transportation-health-data/. Accessed November 13, 2019.

Herron J, Hutchinson R, Lecky F, Bouamra O, Edwards A, Woodford M, Eardley WGP. The impact of age on major orthopaedic trauma: an analysis of the United Kingdom Trauma Audit Research Network database. *Bone Joint J.* 2017;99-B(12):1677–1680.

Lid IM. Developing the theoretical content in Universal Design. *Scandinavian Journal of Disability Research*. 2013;15(3):203–215.

Morris JN, Hardman AE. Walking to Health. *Sports Medicine*. 1997;23(5):306–332.

NCHS, CDC. International Classification of Diseases, Ninth Revision, Clinical Modification. 2015. Available at: https://www.cdc.gov/nchs/icd/icd9cm.htm. Accessed August 13, 2020.

Retting R. *Pedestrian Traffic Fatalities by State 2019 Preliminary Data*. (Feese J, Martin R, Macek K, eds.). Washington, DC: GHSA; 2020:1–44.

Sandt L, Brookshire K, Stephen H, Blank K, Harmon KH. *Toward a Shared Understanding of Pedestrian Safety: An Exploration of Context, Patterns, and Impacts*. Chapel Hill, NC: PBIC; 2020.

Slavova S, Costich JF, Luu H, Fields J, Gabella BA, Tarima S, Bunn TL. Interrupted time series design to evaluate the effect of the ICD-9-CM to ICD-10-CM coding transition on injury hospitalization trends. *Inj. Epidemiol.* 2018;5(1):36.

Thomas L, Vann M, Levitt D. *North Carolina Pedestrian Crash Types 2012-2016*. Raleigh, NC: Division of Bicycle and Pedestrian Transportation, NC DOT; 2018.

Vespa J, Medina L, Armstrong DM. *Demographic turning points for the United States: Population projections for 2020 to 2060*. Washington, DC: US Census Bureau; 2020.

TABLES

Table 1. Selected characteristics of police-reported pedestrian injuries treated in North Carolina emergency departments, stratified by age group: October 2010 – September 2015

Selected characteristics, N (%)		**Age group**					
		0-14 (N=764)	**15-24 (N=1,567)**	**25-64 (N=4,010)**	**≥65 (N=578)**	**Total (N=6,919)**	***P* value**
Sex							<.001
	Male	478 (62.6)	905 (57.8)	2,318 (57.8)	274 (47.5)	3,975 (57.5)	
	Female	286 (37.4)	661 (42.2)	1,689 (42.2)	303 (52.5)	2,939 (42.5)	
Race/Ethnicity							<.001
	White	248 (32.8)	633 (41.1)	1,858 (47.0)	403 (70.8)	3,142 (46.1)	
	Black/African-American	398 (52.6)	778 (50.5)	1,765 (44.6)	139 (24.4)	3,080 (45.1)	
	Other race/ethnicity[1]	111 (14.7)	130 (8.4)	333 (8.4)	27 (4.7)	601 (8.8)	
Crash location[2]							<.001
	Trafficway	592 (77.5)	1,262 (80.8)	2,807 (70.1)	295 (51.0)	4,956 (71.7)	
	Non-trafficway	172 (22.5)	300 (19.2)	1,197 (29.9)	283 (49.0)	1,952 (28.3)	
Rurality[3]							.002
	Urban (>70% developed)	543 (71.1)	1,133 (72.3)	2,946 (73.5)	457 (79.1)	5,079 (73.4)	
	Mixed (30% -70% developed)	122 (16.0)	228 (14.6)	527 (13.1)	76 (13.1)	953 (13.8)	
	Rural (<30% developed)	99 (13.0)	206 (13.1)	537 (13.4)	45 (7.8)	887 (12.8)	
Estimated driver speed at impact							<.001
	≤35 MPH	621 (84.3)	1,149 (77.1)	3,006 (79.0)	494 (89.8)	5,270 (80.1)	
	>35 MPH	116 (15.7)	342 (22.9)	799 (21.0)	56 (10.2)	1,313 (19.9)	
Ambient light							<.001
	Daylight	554 (72.6)	769 (49.3)	2,157 (54.0)	447 (77.9)	3,927 (56.9)	
	Dawn/Dusk	62 (8.1)	77 (4.9)	169 (4.2)	25 (4.4)	333 (4.8)	
	Dark[4]	147 (19.3)	715 (45.8)	1,672 (41.8)	102 (17.8)	2,636 (38.2)	
Admitted/Died[5]							<.001
	Admitted/Died	144 (18.8)	213 (13.6)	642 (16.0)	152 (26.3)	1,151 (16.6)	
	Discharged/Other disposition	620 (81.2)	1,354 (86.4)	3,368 (84.0)	426 (73.7)	5,768 (83.4)	

Abbreviations: MPH, miles per hour.
Missing: Sex (n=5); race (n=96); crash location (n=11); driver speed at impact (n=336); ambient light (n=23).
[1]Other race/ethnicity consists of patients with American Indian/Native American race, Asian race, and Hispanic/Latino ancestry (Race/ethnicity are not disaggregated in NC crash data).
[2]In NC, investigating law enforcement officers are not required to report crashes on non-trafficways (e.g. parking lots); however, if these events were reported, they were included in analyses.
[3]Rurality was determined by the investigating law enforcement officer.
[4]Consists of pedestrians injured under dark-lighted conditions, dark-unlighted conditions, and dark other/unknown conditions.
[5]A patient received a status of admitted or died if they were admitted to the ED, died in the ED, or were listed as killed on the linked crash report.

Table 2. Location of injury among police-reported pedestrian injuries treated in North Carolina emergency departments, stratified by age group: October 2010 – September 2015[1,2]

Location of injury, N (%)	Age group					
	0-14 (N=764)	15-24 (N=1,567)	25-64 (N=4,010)	65+ (N=578)	Total (N=6,919)	*P* value
Head	302 (39.5)	428 (27.3)	996 (24.8)	193 (33.4)	1,919 (27.7)	<.001
SC/VC	29 (3.8)	163 (10.4)	497 (12.4)	73 (12.6)	762 (11.0)	<.001
Torso	147 (19.2)	303 (19.3)	840 (20.9)	124 (21.5)	1,414 (20.4)	.415
Upper extremity	187 (24.5)	480 (30.6)	1,168 (29.1)	192 (33.2)	2,027 (29.3)	.003
Lower extremity	351 (45.9)	764 (48.8)	1,836 (45.8)	253 (43.8)	3,204 (46.3)	.124

Abbreviations: SC, spinal column; VC, vertebral column.
[1]Location of injury classified according to Barell Injury Diagnosis Matrix.
[2]Pedestrians may have more than one injury diagnosis; therefore, column totals do not sum to 100 percent.

Table 3. Selected injury diagnoses among police-reported pedestrian injuries treated in North Carolina emergency departments, stratified by age group: October 2010 – September 2015[1,2]

Nature of injury, N (%)	Age group					
	0-14 (N=764)	15-24 (N=1,567)	25-64 (N=4,010)	65+ (N=578)	Total (N=6,919)	*P* value
TBI	87 (11.4)	152 (9.7)	319 (8.0)	55 (9.5)	613 (8.9)	.008
Open wound/amputation	112 (14.7)	221 (14.1)	459 (11.4)	93 (16.1)	885 (12.8)	.001
Internal injury[3]	110 (14.4)	197 (12.6)	452 (11.3)	78 (13.5)	837 (12.1)	.051
Fracture	169 (22.1)	358 (22.8)	1,027 (25.6)	197 (34.1)	1,751 (25.3)	<.001
Strain/Sprain/ Dislocation	59 (7.7)	279 (17.8)	751 (18.7)	82 (14.2)	1,171 (16.9)	<.001
Superficial wound/ contusion	480 (62.8)	938 (59.9)	2,204 (55.0)	311 (53.8)	3,933 (56.8)	<.001

Abbreviations: TBI, traumatic brain injury.
[1]Nature of injury classified according to Barell Injury Diagnosis Matrix.
[2]Pedestrians may have more than one injury diagnosis; therefore, column totals do not sum to 100 percent.
[3]Includes crushing injuries and injuries to the blood vessels and nerves.

Wednesday, October 14th, 2020, 12:10 PM - 12:20 PM EST

The Effect of Chin-to-Chest Contact on Upper Neck Axial Force in UN Regulation No. 129 Frontal Impact Tests of Child Restraint Systems

Author: Costandinos Visvikis, costandinos.visvikis@cybex-online.com
Co-Authors: Christoph Thurn, christoph.thurn@cybex-online.com, Matthias Kettner, matthias.kettner@cybex-online.com, Thomas Müller, thomas.mueller@cybex-online.com

ABSTRACT

Objective: To investigate the effect of chin-to-chest contact on upper neck axial force in UN Regulation No. 129 frontal impact tests of child restraint systems.

Methods: Frontal impact pilot experiments were carried out according to the test procedure in UN Regulation No. 129. Q-Series child dummies were seated in a small convenience sample of forward-facing child restraint systems. The timing and duration of chin-to-chest contact were determined using the procedure for calculating external head impact force in SAE J2052.
Results: Chin-to-chest contact was observed in all of our experiments and generated a tensile peak in the upper neck axial force of the Q-Series dummies. Prior to chin-to-chest contact, a purely inertial, non-contact peak was observed in the axial tension force. The tensile peak due to chin-to-chest contact was often greater than the inertial, non-contact peak force.
Conclusions: Chin-to-chest contact can increase axial neck tension force beyond the level it would reach under purely inertial loading. Adopting upper neck axial force in regulation, without considering how the force is generated, might encourage child restraint designs that mitigate only chin-to-chest contact, rather than the true inertial neck loading.

INTRODUCTION

United Nations (UN) Regulation No. 129 specifies Q-Series dummies to assess the performance of child restraint systems in dynamic impact tests. The upper neck tension force and flexion moment are currently measured "for monitoring purposes", but no thresholds are applied. However, the UN Working Party on Passive Safety (GRSP) is considering introducing neck thresholds for the frontal impact test in a future amendment of the regulation (United Nations, 2019). As the test set-up for frontal impact comprises a test bench only, without any structure representing the vehicle interior, the neck measurements are exclusively non-contact forces and moments that assess the risk of inertial neck injury.

The ability of child dummies to predict non-contact, inertial neck injury is a topic of research that has not been addressed fully in any child restraint system regulation. Two main issues have emerged: firstly, the stiff thoracic spine of child dummies results in high neck forces and moments that are not representative of the true injury potential (Sherwood et al., 2003); and secondly, chin-to-chest contact can increase the neck forces and moments beyond the purely inertial peak (Sherwood et al., 2003; Sochor et al., 2006). Furthermore, in the case of the Q-Series, there are no neck injury assessment reference values from which to derive regulatory thresholds (Johannsen et al., 2012).

In the absence of readily-available reference values for the Q-Series, GRSP is investigating whether the "monitoring" data collected during UN Regulation No. 129 type-approval tests can be used to establish pragmatic neck thresholds. This approach also avoids the problem of the dummy (and its stiff thoracic spine) over-estimating the risk of neck injury, since such thresholds would not be linked to the human response directly. However, the potential for chin-to-chest contact to skew the neck forces and moments would still remain and has not previously been investigated for the Q-Series. Such contact has been observed with these dummies, but research has tended to focus on its effect on chest deflection (Visvikis et al., 2013; Pitcher et al., 2015). Thus, the objective of this study was to investigate the effect of Q-Series chin-to-chest contact on upper neck loading in child restraints exposed to the UN Regulation No. 129 frontal impact test.

METHODS

Four frontal impact pilot experiments were carried out on an acceleration sled. Two types of child restraint system were used; a forward-facing ISOFIX seat with a support leg and integral

five-point harness and an ISOFIX booster seat (with backrest). In each case, two experiments were carried out, comprising the upper and lower limit dummies according to the child usage range declared for each seat. The test matrix is shown in Table 1.

All experiments followed the frontal impact test procedure in the 03 series of amendments to UN Regulation No. 129. The regulatory front impact test conditions comprise an impact speed of 52^{+0}_{-2} km/h and an acceleration corridor that peaks between 20 g and 28 g. The dummies were instrumented in the head, neck, chest, abdomen and pelvis and were equipped with a hip liner. All measurement and data analysis conformed to ISO 6487. The timing and duration of chin-to-chest contact were determined using the procedure for calculating external head force in SAE J2052. The procedure uses the head mass (above the neutral axis of the upper neck load cell), the head acceleration components (a_x, a_y, a_z) and the neck force components (F_x, F_y, F_z) in a root sum square calculation. A contact is assumed to have occurred when the external head force level has reached 500 N. High speed cameras captured top, left and oblique views of the dummies during each impact event.

RESULTS

Chin-to-chest contact was observed in all four experiments. In each case, the dummy displayed significant cervical spine flexion with the chin striking the chest in the sternum area. The timing of the contact, and the peak upper neck tension force are provided in Table A1 in Appendix A. Figures 1 and 2 show the upper neck axial force overlaid with the external head contact force in each experiment in the ISOFIX integral seat. Figures A1 and A2 show the same for the ISOFIX booster seat.

The upper neck axial force was influenced by chin-to-chest contact. In each experiment, there was an initial tensile peak prior to chin-to-chest contact, followed by a second peak during the period of contact. The onset of this second peak corresponded with the time of engagement between the chin and chest, identified from the external head impact force. The initial tensile peak was broadly similar in magnitude for each child restraint and/or dummy type. However, the peak due to chin-to-chest contact was more variable. This second peak was the overall peak value in the experiments with the Q1.5 in an ISOFIX integral seat (Figure 1) and with the Q3 and Q10 in an ISOFIX booster seat (Figures A1 and A2 respectively). However, the initial tensile peak was the overall peak value with the Q3 in the ISOFIX integral seat (Figure 2).

DISCUSSION

Chin-to-chest contact generated a tensile peak in the upper neck axial force of the Q-Series dummies. This comprised the overall peak tension in three of our four experiments (see Figures 1, A1 and A2). Similar findings have been observed in other child dummies, including the P-Series (Jansen et al., 1991) and the Hybrid III (Sherwood et al., 2003; Sochor et al., 2006). Although it wasn't possible to investigate in our limited pilot study, it appears that dummy posture and child restraint design can influence chin-to-chest contact characteristics (Klinich et al., 2008; Stammen and Sullivan, 2008). Chin-to-chest contact has also been observed in child cadavers (Sherwood et al., 2003) and in human body models (Maheshwari et al., 2018). However, the severity of contact and its effect on neck forces seems to be much greater in dummies, primarily due to the stiffness of their components (Stammen et al., 2013). Reducing the contact stiffness has been shown to reduce peak neck tensile forces in MADYMO

simulations of a P3/4 dummy (Jansen et al., 1991). Furthermore, the Hybrid III 10 year old dummy chin specifications were tuned to mitigate some of the effects of chin-to-chest contact (NHTSA, 2012). Unfortunately, the prevalence of chin-to-chest contact in real world collisions and its effect on child injury potential, if any, does not appear to have been reported.

Adopting upper neck axial force in regulation, without considering how the force is generated, might serve only to incentivise child restraint designs that mitigate chin-to-chest contact, rather than the true inertial neck force. This might have unintended consequences, not only for inertial neck injury risk, but also that of other body regions. One option would be to exclude the period of chin-to-chest contact from the axial neck force measurement. This might yield the true inertial neck tension force. However, in at least one of our experiments (see Figure A2) the neck force was increasing, beyond the initial peak, prior to chin-to-chest contact. In this case, the dummy chin-to-chest interaction may have masked a more moderate increase in the inertial neck tension force.

In conclusion, chin-to-chest contact can increase axial neck tension force in Q-Series dummies beyond the level it would reach under purely inertial loading. Although real-world and cadaver data are limited, this appears not to be a desirable characteristic of the dummy. The potential for measures to improve the behaviour of the Q-Series will be explored in a further phase of our study. This will encompass a broader range of child restraints and Q-Series dummies and will investigate all potential neck measurement parameters.

ACKNOWLEDGEMENTS
The authors thank the impact test laboratory staff for their technical support in this study.

REFERENCES
Jansen EG, Nieboer JJ, Verschut R, Huijskens CG. Cervical spine loads induced in restrained child dummies. SAE Transactions. 1991;100:2093-113.
Johannsen H, Trosseille X, Lesire P, Beillas P. Estimating Q-dummy injury criteria using CASPER project results and scaling adult reference values. IRCOBI Conf Proc. 2012:580-596.
National Highway Traffic Safety Administration (NHTSA). Hybrid III 10-year-old child test dummy – Final rule. 2012; 77 FR 11651 (NHTSA-2011-0175).
Maheshwari J, Duong N, Sarfare S, Belwadi A. Evaluating the response of the PIPER scalable human body model across child restraining seats in simulated frontal crashes. Traffic Inj Prev. 2018 19:sup2, S140-S142.
Pitcher M, Carroll J, Broertjes P. Research findings for setting dummy injury thresholds for Regulation 129 phase 2 regarding chest and abdomen loading. Proc Int Conf Protection of Children in Cars, 2015.
Sherwood CP, Shaw CG, Van Rooij L, Kent RW, Crandall JR, Orzechowski KM, Eichelberger MR, Kallieris D. Prediction of cervical spine injury risk for the 6-year-old child in frontal crashes. Traffic Inj Prev. 2003 Sep;4(3):206-13.
Sochor MR., Faust DP, Anderson KF, Barnes S, Ridella SA, Wang SC. Assessment of 3 and 6-year-old neck injury criteria based on field investigation, modeling, and sled testing. SAE Transactions. 2006;115:183-209.
Stammen JA, Bolte JH, Shaw J. Biomechanical impact response of the human chin and manubrium. Ann Biomed Eng. 2012 Mar;40(3):666-78.

Stammen JA, Sullivan LK. Development of a Hybrid III 6yr. old and 10 yr. old dummy seating procedure for booster seat testing. National Highway Traffic Safety Administration (NHTSA) Technical Report. 2008; NHTSA Docket 2007-0048-0002.
United Nations. Report of the Working Party on Passive Safety on its sixty-fifth session. Geneva, 13-17 May 2019. Available at: https://undocs.org/ECE/TRANS/WP.29/GRSP/65.
Visvikis C, Carroll J, Picher M, Barrow A, Cuerden R, Broertjes P. Research findings for the optimised evolution of the new regulation on enhanced child restraint systems. Proc Int Conf Protection of Children in Cars, 2013.

APPENDIX A

Table A1: Chin-to-chest contact period, according to the procedure specified in SAE J2502, and upper neck tension force peak and time of peak

Child restraint system	Dummy	Chin-to-chest contact period		Neck tension force	
		Begin contact (ms)	End contact (ms)	Peak (N)	Time (ms)
ISOFIX integral seat	Q1.5	85.1	112.5	1728.4	94.2
	Q3	83.8	123.8	1933.1	78.2
ISOFIX booster seat	Q3	80.3	115.1	2628.1	88.2
	Q10	87.0	128.9	3846.4	98.7

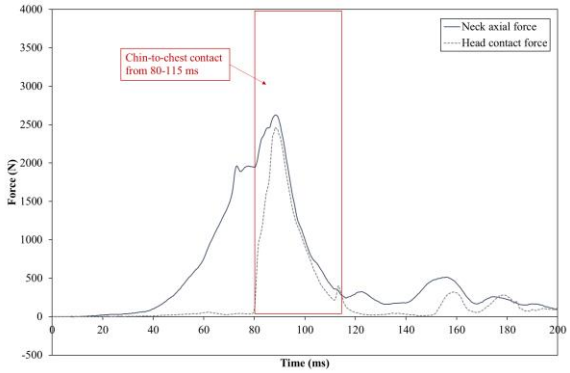

Figure A1: Upper neck axial force and head contact force with Q3 dummy in ISOFIX booster seat

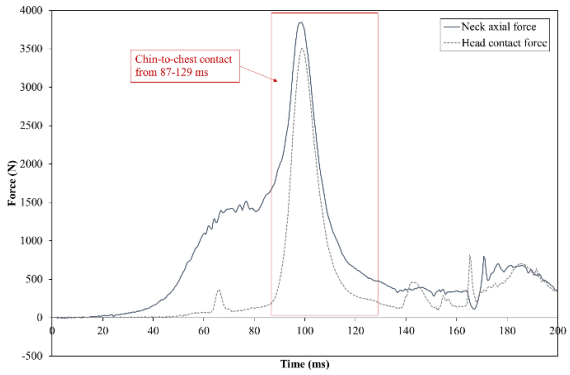

Figure A2: Upper neck axial force and head contact force with Q10 dummy in ISOFIX booster seat

TABLES AND FIGURES

Table 1: Test matrix

Child restraint system	Dummy Q1.5	Q3	Q10
ISOFIX integral	✓	✓	
ISOFIX booster		✓	✓

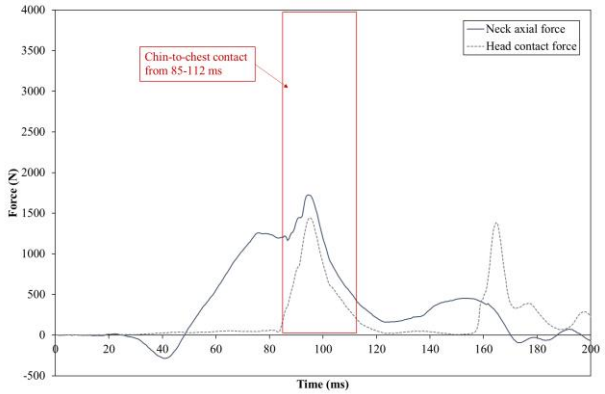

Figure 1: Upper neck axial force and head contact force with Q1.5 dummy in ISOFIX integral seat

Wednesday, October 14th, 2020, 12:20 PM - 12:30 PM EST

Pedestrian injuries from cars and SUVs: Updated crash outcomes from the Vulnerable Road User Injury Prevention Alliance (VIPA)

Author: Samuel Monfort, smonfort@iihs.org
Co-Author: Becky Mueller, bmueller@iihs.org

ABSTRACT

Objective: The current short communication was written to update research on real-world pedestrian crashes. In particular, our analysis offers a preliminary update on SUV-pedestrian crash outcomes and how they differ from car-pedestrian crash outcomes. Detailed injury data were linked to vehicle features to offer a better understanding of pedestrian injury etiology.

Methods: We analyzed 82 single-vehicle crashes from the VIPA pedestrian crash database, focusing on crashes involving an SUV or car. Each crash from this database includes an in-depth analysis of police reports, pedestrian medical records, crash reconstructions, and injury attribution by a panel of experts.

Results: SUVs remain disproportionately likely to injure and kill pedestrians compared with cars, but these differences emerged primarily at crashes of intermediate speed. Crashes at low speeds and high speeds tend to produce similar injury outcomes independent of striking vehicle type (mild and fatal, respectively) The data suggest that the elevated danger to pedestrians from SUVs in these crashes may be largely related to injuries caused by impacts with the vehicles' leading edge: the bumper, grille, and headlights.

Conclusions: Although the current analysis was based on a non-nationally representative dataset, the elevated pedestrian injury risk originating from SUVs' leading edge is consistent with past research on the subject. That is, despite the changes in vehicle design and fleet composition over the past two decades, SUVs may remain disproportionately likely to injure pedestrians compared with cars.

INTRODUCTION

Annual pedestrian fatalities have increased nearly every year since 2009, and the rate per 100,000 people observed in 2018 was at its highest since 1998. In fact, pedestrians now account for 17% of all traffic fatalities, a proportion unseen since 1982.[1,2] Past research has found that SUVs, pickup trucks, and passenger vans pose an outsize risk to pedestrians. Compared with cars, these vehicles (collectively known as LTVs) are 2-3 times more likely to kill the pedestrian in a crash.[3,4] The elevated injury risk associated with LTVs seems to stem from their higher leading edge, which tends to impart greater injury to the middle and upper body (including the thorax and abdomen) than cars, which instead tend to cause injury to the lower extremities.[5-7]

The objective of the current study was to offer a preliminary update on SUV-pedestrian crash outcomes and how they differ from car-pedestrian crash outcomes. To date, research on real-world pedestrian crash outcomes has largely been restricted to two NHTSA datasets: the Pedestrian Injury Causation Study (PICS) from 1977 and the Pedestrian Crash Data Study (PCDS) from 1994. Vehicle design and fleet composition have changed substantially in the decades since these two data collections were completed.[8] In particular, SUVs have adopted more car-like features in the intervening decades (e.g., unibody construction and a lower center of gravity). Although these changes have contributed to a lower risk to occupants of cars in collisions with SUVs, single-vehicle pedestrian fatalities involving SUVs have increased more than those involving other vehicle types over the past decade.[9] Understanding the pedestrian risk factors unique to the modern SUV fleet is important for informing how these vehicles are designed going forward.

METHODS

VIPA pedestrian crash data were collected by the International Center for Automotive Medicine Pedestrian Consortium. The consortium began data collection in 2015, producing a detailed database of Michigan pedestrian and bicyclist crashes where police were called to the scene. These data are not necessarily nationally representative, but include an in-depth analysis of police reports, scene information, medical records, crash reconstructions, and injury attribution by a panel of experts. The median model year for involved vehicles was 2009 (SD=5 years). Pickup crashes were excluded because there were too few in the dataset to support valid conclusions. The current study focused on the 79 completed pedestrian crashes involving exactly one pedestrian over the age of 13 and one SUV (n=24) or car/minivan (n=55) and the injury analyses were conducted using the single most severe injury for each pedestrian. Injuries were coded using the 2005/2008 Abbreviated Injury Scale (AIS) and Injury Severity Score (ISS), the squared sum of the three highest AIS scores.

RESULTS

Controlling for preimpact speed, as well as pedestrian age, gender, and weight, we found SUVs to cause significantly more severe pedestrian injuries than cars did (p=.003; median ISS 17 vs. 9). The discrepancy in pedestrian injury outcomes between cars and SUVs was largest at higher preimpact speeds. In fact, pedestrians struck at 19mph or slower exhibited roughly similar outcomes regardless of the striking vehicle type. Preimpact speeds exceeding 19mph, however, produced substantially worse injury outcomes for pedestrians struck by SUVs than by cars (Figure 1). This effect was generally mirrored by fatality rates in struck pedestrians (Figure 2).

Consistent with past research,[7] SUVs were more likely to throw struck pedestrians forward than cars were (36% vs. 26%). Pedestrians struck by SUVs were also nearly twice as

likely to be severely injured in the thigh/hip compared with pedestrians struck by cars (24% of all SUV crashes resulted in AIS 3+ injuries compared with just 16% for cars). Severe thigh/hip injuries for pedestrians struck by SUVs were disproportionately caused by impacts with features on those vehicles' leading edges: the bumper, the grille, or the headlights (Figure 3).

DISCUSSION

Despite the changes in vehicle design over the past two decades, SUVs remain disproportionately likely to injure pedestrians compared with cars. Interestingly, the danger that SUVs pose to pedestrians seems to be most pronounced in crashes where the striking vehicle was traveling faster than 19 miles per hour. The data suggest that crash characteristics tend to overpower vehicle characteristics for low-speed crashes. That is, low-speed crashes tend to be benign enough that pedestrians emerge with only minor injuries regardless of vehicle type. Crashes at faster speeds are where vehicle design differences begin to predict injury outcomes.

Although recent vehicle crash data suggest that being struck by an SUV while driving a car is now equivalent to being struck by another car,[8,10] the same equivalence may not apply to being struck while walking. Of note, the VIPA data are not necessarily nationally representative, as crashes were only collected from three urban areas in Michigan. As a result, the conclusions presented in the current short communication should be considered preliminary until a more diverse dataset can be compiled. Future research should investigate whether the findings contained in the current short communication can be replicated in a more generalizable set.

Limited generalizability notwithstanding, the detailed injury data in the VIPA database revealed that the elevated danger to pedestrians from SUVs may be largely related to injuries caused by high-speed impacts with the vehicles' leading edge. In all, the data suggest that despite improvements in vehicle crash compatibility, SUVs may remain more disproportionately dangerous to pedestrians.

ACKNOWLEDGEMENTS

The authors would like to acknowledge the contribution of the International Council for Automotive Medicine Vulnerable Road Users Prevention Alliance members: Susan Owen at General Motors; Tim Keon at Subaru Corporation; Nick Ables at Hyundai Motor Group; Jason Gainey at Volkswagen Group of America; Anja Schneider at Audi AG, Global Safety Affairs,; and Stuart Wang, Kristen Cunningham, Carla Kohoyda-Inglis, and Robert Kaufman at ICAM.

REFERENCES

1. Insurance Institute for Highway Safety. Fatality facts 2018: Pedestrians. Available at: https://www.iihs.org/topics/fatality-statistics/detail/pedestrians. Accessed April 14, 2020.
2. Retting R. Pedestrian traffic fatalities by state: 2019 preliminary data. Governors Highway Safety Association. Available at: https://www.ghsa.org/resources/Pedestrians20. Published February 2020. Accessed April 14, 2020.
3. Lefler D, Gabler HC. The fatality and injury risk of light truck impacts with pedestrians in the United States. *Accid Anal Prev*. 2004;36:295-304. doi:10.1016/s0001-4575(03)00007-1
4. Roudsari BS, Mock CN, Kaufman, R, Grossman D, Henary BY, Crandall J. Pedestrian crashes: Higher injury severity and mortality rate for light truck vehicles compared with passenger vehicles. *Inj Prev*. 2004;10(3):154-158. doi:10.1136/ip.2003.003814
5. Ballesteros M, Dischinger P, Langenberg, P. Pedestrian injuries and vehicle type in Maryland, 1995–1999. Accid Anal Prev. 2004;36:73-81. doi:10.1016/s0001-4575(02)00129-x

6. Longhitano D, Henary B, Bhalla K, Ivarsson J, Crandall J. *Influence of vehicle body type on pedestrian injury distribution*. Technical paper 2005-01-187. SAE International. Published April 11, 2005. doi:10.4271/2005-01-1876
7. Roudsari BS, Mock CN, Kaufman R. An evaluation of the association between vehicle type and the source and severity of pedestrian injuries. *Traffic Inj Prev*. 2005;6(2):185-192. doi:10.1080/15389580590931680
8. Monfort SS, Nolan JM. Trends in aggressivity and driver risk for cars, SUVs, and pickups: Vehicle incompatibility from 1989 to 2016. *Traffic Inj Prev*. 2019;20:S92-S96. doi:10.1080/15389588.2019.1632442
9. Hu, W, Cicchino, JB. An examination of the increases in pedestrian motor-vehicle crash fatalities during 2009-2016. *J Safety Res*. 2018;67:37-44. doi:10.1016/j.jsr.2018.09.009
10. Teoh ER, Nolan JM. Is passenger vehicle incompatibility still a problem? *Traffic Inj Prev*. 2012;13(6):585-591. doi:10.1080/15389588.2012.676222

FIGURES

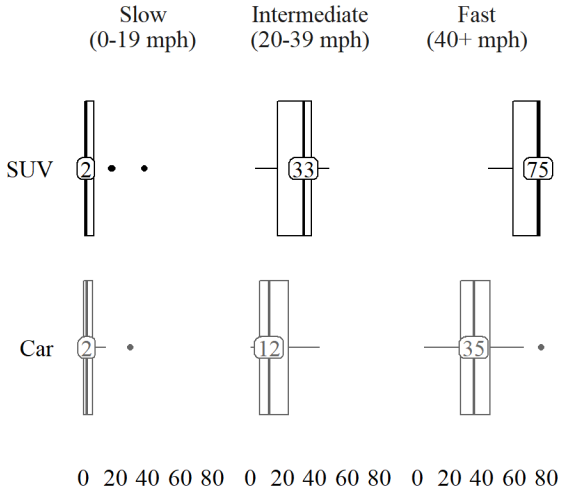

Figure 1. ISS by preimpact speed and striking vehicle type

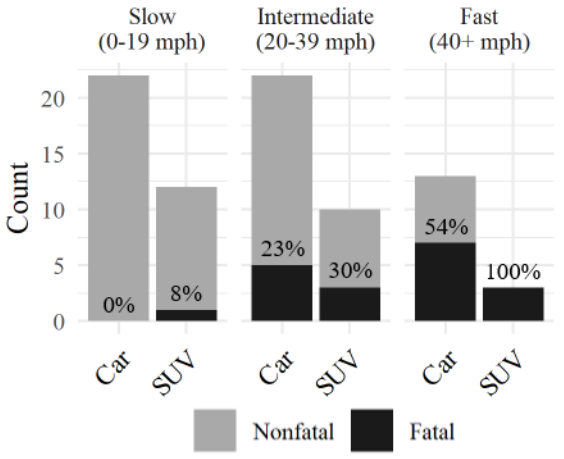

Figure 2. Pedestrian fatality rate by striking vehicle type and preimpact speed.

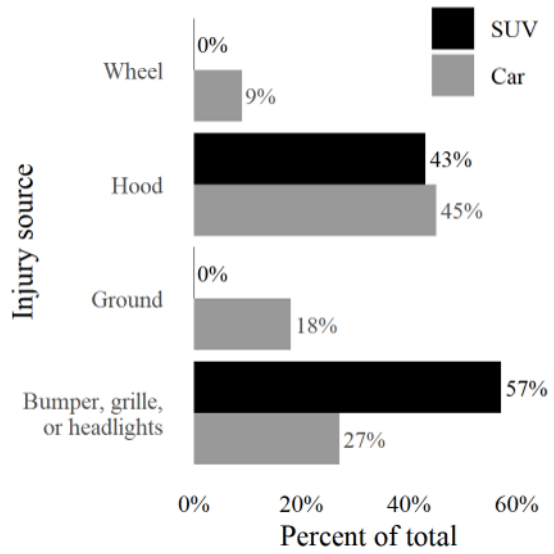

Figure 3. Source of AIS 3+ high/hip injury by striking vehicle type

Wednesday, October 14th, 2020, 1:15 PM - 1:25 PM EST
Development and Validation of an Elderly Human Body Model for Frontal Impacts
Author: Sagar Umale, sumale@mcw.edu
Co-Authors: Prashant Khandelwal, pkhandelwal@mcw.edu, John Humm, jhumm@mcw.edu
Narayan Yoganandan, yoga@mcw.edu

ABSTRACT

Objective: The study aims to develop an elderly model occupant representative of 50th percentile 75-year-old male using the younger 50th percentile Global Human Body Models Consortium Human Body Model.
Methods: The 50th percentile base model was morphed to elderly anthropometry. The material properties of tissues were updated according to the aging functions from the literature. The elderly model was simulated for thoracic impact, abdomen impact, and frontal impact sled tests. The model-predicted contact force-displacement, regional body excursion, acceleration, and seatbelt force responses were compared with matched elderly postmortem human surrogate experimental data.
Results: The force-displacement responses for the thorax and abdomen impacts were within the experimental corridors. The head excursion in the z-direction was within the mean ± one standard deviation experimental corridors. The correlation analysis values of the head, T1 vertebra, pelvis acceleration, and seatbelt forces signals for the frontal sled tests were 0.62, 0.72, 0.63, and 0.78, respectively, and the overall mean value was 0.69.
Conclusions: The developed model with the morphological and material changes representing an elderly occupant is considered to be validated under three experimental scenarios, and it can be used for crashworthiness applications (develop countermeasures) with a focus on elderly

occupants. The process used in the development of the elderly model can also be used to understand the responses of elderly occupants with different postures.

INTRODUCTION

The elderly population in the United States is increasing (Vincent 2010) and so is their vehicle occupancy. Aging increases the likelihood of impact injuries and their consequences, including fatalities; thus, countermeasures might need to be updated for this population. Traditionally, experiments using postmortem human surrogates (PMHS) are performed to determine occupant kinematics; however; finite element human body models are effective because of their repeatability and reproducibility. The 50th percentile 26-year-old Global Human Body Models Consortium Human Body Model, GHBMC (Schoell 2015), and Total Human Model for Safety (Kent 2005) were used to develop elderly occupant models. The emphasis was to update the thoracic morphology and material properties for the elderly. However, the spine curvature and sitting posture change with age (Reed 2012), leading to alterations in the occupant kinematics. These factors were not taken into consideration in these models. The aims of the present study, therefore, was to develop an elderly model using the 50th percentile male GHBMC model that accounts for anthropometric, posture and material properties, and validate the model under frontal impacts, using elderly-specific PMHS experiments.

METHODS

Development of the elderly model: The GHBMC base model was morphed to the elderly surface geometry (structure: 172.6 cm, BMI: 29, age: 75 years) obtained from an occupant posture database (humanshape.org). The hexahedral morph box (hex-box) technique was used for morphing. The hex-boxes were developed for the base model (Figure 1). The spine was encapsulated in the innermost layer of the hex-boxes, and the outermost layer surrounded the head, thorax, and limbs. An intermediate layer of hex-boxes in the thorax surrounded organs like the heart, lungs, liver, and other fat tissue, along with the rib cage and intercostal muscles. The elderly occupant surface geometry and the baseline model were aligned at the H-point. The edges and corners of the hex-boxes were mapped to the elderly geometry, and the elements enclosed in the boxes were morphed to the elderly occupant (Figure 1). The difference in the rib angle between a 26-year-old and a 75-year-old was calculated (Kent 2005), and the ribs were rotated 7 degrees upwards. The neck was rotated to match the kyphotic neck of the elderly. A rigid constraint was applied to maintain the shape of all hard tissues during morphing. The material properties of the hard and soft tissues were updated for the elderly based on the literature.

Validation of the elderly model: The developed elderly model was validated using PMHS experimental data for the thoracic impact (Kroell 1971, 1974), abdomen impact (Hardy 2001), and frontal impact sled tests (Pintar 2010). The average PMHS ages were 72±6 years for the thorax impact, 75±9 years for the abdomen impact, and 78±6 years for the frontal impact sled tests. Two thoracic impacts with impactor mass of 10.4 kg and 23.6 kg and 152.4 mm diameter at 7m/s, to the sternum along the midsagittal plane were simulated. Two abdomen impacts were simulated at the L3 level using 25 mm and 48 kg bar at 6 m/s and 9m/s. The contact force and displacement of the impactors were compared with experimental results. The frontal impact simulation environment consisted of a rigid seat, footrest, B-Pillar and seatbelt anchors. The elderly model was positioned on the seat and restrained with a 3-point seatbelt. An initial velocity of 6.7 m/s and a frontal deceleration pulse of 17 g was applied to the environment. The

head excursion, resultant head, T1, and pelvis accelerations and seatbelt force of the elderly model were compared with experimental results. Correlation and analysis (CORA) methods were used to quantify the goodness-of-fit between simulation and experimental responses.

RESULTS

The contact force and displacement for the thorax (for both impact masses) and abdomen (for both velocities) impacts were within the experimental corridors (Figure 2). The stiffness, defined as the slope of the force-displacement curve, of the thorax was bilinear. For the 10 kg impactor, the chest stiffness was 78 kN/mm until 30 mm of chest deformation, and 6 kN/mm between 30 mm and 90 mm of chest deformation. For the 23 kg impactor, the chest stiffness was 80 kN/mm until 30 mm of chest deformation, and 22.5 kN/m between 30 mm and 90 mm of chest deformation. The abdomen stiffness was 49.2 kN/m and 29.8 kN/m for 9 m/s and 6 m/s impactors. In the sled tests, the head excursion in x and z directions were 155 mm and 297 mm. The average CORA for the simulation response (head, T1, pelvis accelerations and seatbelt forces) was 0.69 (Figure 2).

DISCUSSION

In this study, an elderly male human body model representative of a 75-year-old occupant in terms of mass and stature was developed and validated using elderly experimental data. The morphology and posture of the elderly occupant were achieved by morphing the base model using a novel hex-box technique. The thorax and abdominal impact responses were within the experimental corridors. The abdominal stiffness of the elderly model was within the range (50–75 kN/m and 19–35 kN/m for 9m/s and 6m/s) reported in the literature (Hardy 2001; Cavanaugh 1986). In the frontal impact sled test, the head excursion of the elderly model in the z-direction was within one standard deviation from the experimental results (280±80 mm), while it was lesser in the x-direction (185±4 mm). The lower x excursion was attributed to the more forward head position in the simulation and kyphotic neck. The alignment of the neck was not available from the experimental study. Acknowledging these features, the developed elderly model is considered to reasonably represent the elderly population. As a first step, it can be used in crashworthiness studies and develop countermeasures.

ACKNOWLEDGMENTS

The study was supported by the US DOT DTNH2217R00065. The authors thank the Global Human Body Models Consortium for providing the model and the Neuroscience Laboratories personnel at MCW.

REFERENCES

1. Cavanaugh, J. M., Nyquist, G. W., Goldberg, S. J., King, A. I. 1986. 'Lower Abdominal Tolerance and Response', 30th Stapp Car Crash Conference, SAE Technical Paper 861878.
2. Hardy, W. N., Schneider, L. W., Rouhana, S. W. 2001. 'Abdominal impact response to rigid-bar, seatbelt, and airbag loading', Stapp Car Crash J, 45: 1-32.
3. Kent, R., Lee, S. H., Darvish, K., Wang, S., Poster, C. S., Lange, A. W., Brede, C., Lange, D., Matsuoka, F. 2005. 'Structural and material changes in the aging thorax and their role in crash protection for older occupants', Stapp Car Crash J, 49: 231-49.
4. Kroell, Charles K., Schneider, D. C., Nahum, A. M. 1971. "Impact Tolerance and Response of the Human Thorax." In.: SAE International.

5. ———. 1974. "Impact Tolerance and Response of the Human Thorax II." In.: SAE International.
6. Pintar, F. A., Yoganandan, N., Maiman, D. J. 2010. 'Lower cervical spine loading in frontal sled tests using inverse dynamics: potential applications for lower neck injury criteria', Stapp Car Crash J, 54: 133-66.
7. Reed, M.P., Ebert-Hamilton, S.M., Rupp J.D. 2012. 'Characterizing Posture, Body Shape and Belt Fit for Older Occupants ', Stapp Car Crash J, Shot Communication.
8. Schoell, S. L., Weaver, A. A., Urban, J. E., Jones, D. A., Stitzel, J. D., Hwang, E., Reed, M. P., Rupp, J. D., Hu, J. 2015. 'Development and Validation of an Older Occupant Finite Element Model of a Mid-Sized Male for Investigation of Age-related Injury Risk', Stapp Car Crash J, 59: 359-83.
9. Vincent, Grayson K., Velkof, V. A. 2010. 'THE NEXT FOUR DECADES The Older Population in the United States: 2010 to 2050', U.S. Department of Commerce Economics and Statistics Administration, U.S. CENSUS BUREAU.

Figure1. Morph boxes developed for base (left) and morphed elderly model (right)

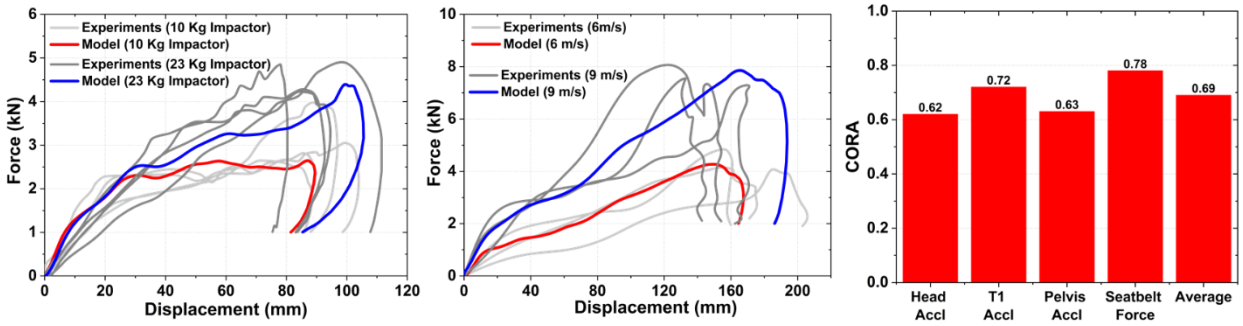

Figure 2. Comparison of force vs displacement data for (left) thorax and (middle) abdomen impacts, and CORA values (right) for sled test responses.

Thursday, October 15th, 2020
2:00 PM - 3:25 PM: Pre-/Post-Crash Research

Thursday, October 15th, 2020, 2:30 PM - 2:40 PM EST
Video from User-Generated Content as a Source of Pre-Crash Scenario Naturalistic Driving Data
Author: Schuyler St. Lawrence, schuyler.stlawrence@toyota.com
Co-Authors: Jason Hallman, jason.hallman@toyota.com, Rini Sherony, rini.sherony@toyota.com

ABSTRACT
Objective: The objective of this study was to investigate the use of public video from internet user-generated content as a means of collecting naturalistic driving data.
Methods: A convenience sample of 38 videos comprised of 203 events was extracted from publicly available channels on the YouTube™ platform. Each event was manually reviewed and pseudo-coded according to a subset of current CRSS variables. Pre-crash scenarios were coded using categories developed for prior NHTSA analysis.
Results: Crashes represented 67% of the reviewed cases. Collisions with motor vehicles accounted for 84% of all crashes in the sample. Pre-crash scenarios were able to be determined for all crashes and near-crashes. The most prevalent pre-crash scenario types in the video data were Crossing Paths (41%), Rear End (21%), and Lane Change (17%). The top pre-crash scenarios from Swanson et al., were Rear End (31%), Crossing Paths (21%), and Lane Change (12%). The most prevalent pre-near crash scenario types in the video data were Crossing Paths (32%), Lane Change (30%), and Pedestrian (12%).
Conclusions: The most prevalent pre-crash scenarios in the video data were similar to those in data from FARS and NASS-GES. Though not nationally representative, this preliminary study demonstrated that user-generated content may be useful as a source of inexpensive naturalistic data and provides sufficient detail to capture important pre-crash, near-crash and crash information.

INTRODUCTION
According to NHTSA data, crashes of any severity occur at a rate of approximately two per one million vehicle miles traveled (NCSA 2018). Naturalistic driving studies have long been considered one of the best ways to understand crash causation and crash characteristics. Data from previous studies such as NHTSA's 100-Car Naturalistic Driving Study (Dingus et al. 2006) and the second Strategic Highway Research Program, or SHRP 2 (Hankey et al. 2016) have been used to generate important findings for both crash and near-crash scenarios. However, due to the extensive data collection, such studies are costly to undertake, and even the largest include fewer than 5,000 on-road vehicles. In the years since the 100-Car study was conducted, the cost of consumer video cameras has decreased substantially, leading many drivers to equip their own vehicles with forward-facing cameras, or dashcams. This proliferation of on-road cameras has increased the number of vehicle miles traveled in camera-equipped vehicles and allowed for the capture of many crash and near-crash events. Many dashcam owners voluntarily upload event videos to online video-sharing sites, such as YouTube™, or provide their event videos to content

aggregators. User-generated content has been used to analyze rare events, such as robberies (Legewie et al 2018) and vulnerable road user crashes (Han et al 2017). Thus, the goal of this study was to evaluate the usefulness of user-generated event videos for identifying pre-crash and pre-near-crash scenarios, as well as to understand the benefits and limitations of this type of data collection.

METHODS

Video Analysis

A convenience sample of 38 US crash and near-crash event videos was extracted from various YouTube user-generated content. The videos contained 203 individual events. In order to find usable videos, search terms included
"dash cam crashes," "dashcam crash," "dash cam crash usa," "dashcam pedestrian," "dashcam near miss usa," and "automatic emergency braking dashcam." YouTube's suggested related videos were occasionally used. Each event was given a case number based on a partial URL identifier. Data extraction occurred between February and April 2020. The videos included events that occurred between July 6, 2015 and March 30, 2020, though not all event dates were known.

Event Coding

Event videos were categorized as either a "crash" or a "near-crash." The video type was also coded as either "ego vehicle," "third-party vehicle," or "third-party other." The vehicle equipped with the dashcam was considered the "ego vehicle" in each event. Each distinct event was subjectively coded according to a subset of variables from NHTSA's Crash Report Sampling System (NCSA 2018), including crash time, crash type, manner of collision (crashes only), crash direction, vehicle movement, roadway alignment, relation to junction for intersection events, and several others. Vehicle type was recorded when visible. Each event was also coded according to the 36 distinct pre-crash scenarios outlined in Swanson et al (2019). These 36 scenarios were then further combined into nine scenario types: Control Loss, Road Departure, Animal, Pedestrian, Pedalcyclist, Lane Change, Opposite Direction, Rear End, and Crossing Paths. Subjective assessments of crash severity (minor, moderate, severe) and travel speed (low, moderate, high) were also coded. Posted speed limits were noted when available. Date and time of the event were also recorded when available. Finally, brief narratives of each event were written.

RESULTS

Crash Events

Crash events accounted for 67% of the total set of events. Half of the event videos were coded as "ego vehicle" videos and half were from third party sources. Of the 136 crash events, 118 were collisions with another motor vehicle. Daylight crashes accounted for 71% of the crash events. Among all crashes, 80 (59%) were subjectively noted as "minor," 37 (27%) were "moderate," and 19 (14%) were "severe." Twenty-five of the 36 pre-crash scenarios from Swanson et al (2019) were represented in the data. The three most common individual pre-crash scenarios were "left turn across traffic, opposite direction" with 13%, and "Lane Change, Same Direction" and "rear end/lead vehicle decelerating," both with 11%. When combined into the pre-crash scenario types, the most common were "crossing paths" (41%), "rear end," (21%), and "lane change" (17%). The "left turn across path, opposite direction" scenario accounted for more than 25% of

the “severe” crashes. Despite a concerted effort to include pedestrian events, very few pedestrian impacts were found in the sample (2%).

Near-Crash Events

Near crash events accounted for one third of the overall data set. Among these events, 78% of the videos were “ego vehicle” videos. Nearly three-quarters of the events occurred during daylight hours. Fifteen of the 36 pre-event scenarios were represented in the near-crash event data with the most prevalent single scenario being “lane change, same direction,” accounting for 27% of all events. The top three scenario categories for near-crash events were Crossing Paths (32%), Lane Change (30%), and Pedestrian (12%).

DISCUSSION

Figure 1 compares the top three most common pre-crash scenarios from the NASS-GES and FARS analysis carried out by Swanson et al (2019) with both the crash and near-crash events collected for this study. While the top three categories remain primarily consistent, the fractions are somewhat dissimilar. Crossing path crashes are more likely to be found in the video data than in the police reported data, whereas rear end crashes are less likely to appear in the video crash data and much less likely to appear in the video near-crash data. This may be due to the inherent properties of online video sharing. The videos are generally uploaded for entertainment purposes, which likely resulted in self-selection bias and an over-representation of the more dramatic crash types. For example, videos of “left turn across path” scenarios in which the view of the oncoming vehicle is obstructed by other lanes of stopped traffic, so called “pull through turns,” are very common in the video data set. These crashes tend to be more severe and tend to have a “surprise” factor. Minor rear end crashes and rear end near-crashes are very commonplace in the field and thus may not be as interesting to the public when compared to other types of crashes.

In addition to the event descriptions and pre-crash scenarios, other data were capturable in the videos. Posted speed limits appeared in approximately 20% of all event videos and ego vehicle speeds were occasionally shown in the dash cam footage, however the frequency at which the speeds were updated was insufficient to determine the actual vehicle speed at the time of crash. In most videos, there were substantial location indicators, such as street signs, freeway exit numbers/names and places of business. It may be possible to accurately determine the location of the crash in most cases, though this work has not been done. If the location can be determined, the creation of detailed scene diagrams is possible and would allow for verification of roadway feature coding. Finally, in several videos, audible alarms occur immediately prior to the crash or near-crash. These alarms may represent vehicle advanced driver assistance systems (ADAS), but this was not verifiable.

This type of video data collection has several benefits compared to more detailed large-scale naturalistic driving studies. Videos are often posted online quickly, thus the latency from event to public availability can be days rather than months or years. In addition, the data collection is inexpensive, and a large data set of rare event types can be collected quickly. There are also several “channels” on YouTube dedicated to aggregating event videos, which can simplify case collection. The continued proliferation of dashcams on US roadways suggests that the number of available events will continue to increase and may come to more closely represent the true field distribution of crash configurations.

There are many limitations to this type of video convenience sample. No data on driver demographics were available. It is sometimes possible to infer driver behavior from the event video, but the accuracy of such inferences is suspect. There also were no objective data (e.g.

delta-v) to describe crash severity. In general, cases with visible airbag deployment and cases in which at least one vehicle appeared to require towing were considered "severe." The PDOFs of the crashes were also not calculable. The majority of the motor vehicle collision cases were classified as "angle" crashes and descriptions of the location of damage for each vehicle were noted. This data may be able to serve as a rough proxy for PDOF. Ego vehicle type is also undetermined for videos in which the ego vehicle is involved in the event except in cases where post-event still photos are also included. Finally, the relationship between convenience samples and national trends may be difficult to determine and the self-selection of public video data may bias the results.

Future Work

Given the unknown effects of selection bias, which may preclude representative studies, detailed multi-disciplinary case reviews will be conducted for a subset of the events. These case reviews can be used to assess potential ADAS countermeasures that may address the specific event types. In addition to the case reviews, new video data will be collected, coded and cross-coder analyses will be conducted to look at the effects of coding subjectivity. The full set of CRSS variables will also be investigated to determine the proportion that can be reliably coded

REFERENCES

Dingus TA, Klauer SG, Neale VL, et al. The 100-Car Naturalistic Driving Study, Phase II—Results of the 100-Car Field Experiment. Washington, DC: National Highway Traffic Safety Administration; 2006. DOT HS 810 593.

Han Y, Li Q, Wang F, Wang B, Mizuno K, Zhou Q. Analysis of Vulnerable Road User Kinematics Before/During/After Vehicle Collisions Based on Video Records, Paper presented at IRCOBI,13-15 Sep 2017. Antwerp, Belgium.

Hankey JM, Perez MA, McClafferty JA. Description of the SHRP2 Naturalistic Database and the Crash, Near-Crash, and Baseline Data Sets. Task Report. Blacksburg, VA: Virginia Tech Transportation Institute; 2016.

Legewie N, Nassauer A. YouTube, Google, Facebook: 21st Century Online Video Research and Research Ethics. Forum: Qualitative Social Research. 2018; 19(3), Art. 32

National Center for Statistics and Analysis. Crash Report Sampling System CRSS Analytical User's Manual 2016-2018. Washington, DC: National Highway Traffic Safety Administration; 2018. DOT HS 812 846.

National Center for Statistics and Analysis. Traffic Safety Facts 2017. Washington, DC: National Highway Traffic Safety Administration; 2018. DOT HS 812 806.

Swanson E, Foderaro F, Yanagisawa M, Najm WG, Azeredo P. Statistics of Light-Vehicle Pre-Crash Scenarios Based on 2011-2015 National Crash Data. Washington, DC: National Highway Traffic Safety Administration; 2019. DOT HS 812 745

FIGURE

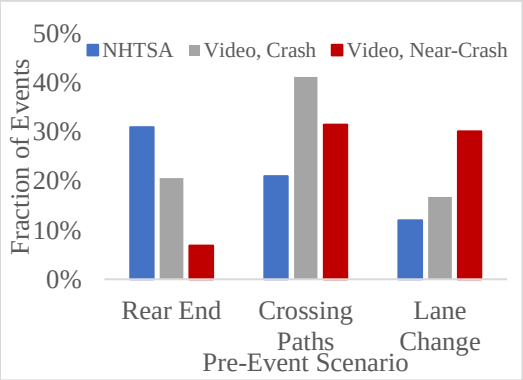

Figure 1. Prevalence of Pre-event Scenario Categories in Video and NHTSA Data

Thursday, October 15th, 2020, 2:40 PM - 2:50 PM EST

Lower Neck Injury Criteria for THOR and Hybrid III Dummies in Rear Impact

Author: Narayan Yoganandan, yoga@mcw.edu
Co-Authors: John Humm, jhumm@mcw.edu, Preston Greenhalgh, preston.c.greenhalgh@nasa.gov, Jeffrey Somers, jeffrey.t.somers@nasa.gov

ABSTRACT

Objective: The objectives of the study are to derive lower-neck-injury probability curves under rear impact loading from matched pair Hybrid III and THOR dummy tests.

Methods: Twelve whole-body and 15 isolated head-neck rear-impact sled tests were conducted using the 2 dummies. They were positioned on a rigid seat that was attached to an acceleration sled. The dummies were positioned with the head parallel to the ground, torso against the seat back, and legs stretched such that there was no axial rotation. The acceleration pulse matched the previous in-house human cadaver tests. The 6-axis lower-neck load cell was used in both dummies. For the isolated rear-impact tests, the head-neck was excised from the dummies, and the lower-neck load cell was mounted to the top of the sled with the head parallel to the ground and such that the acceleration vector was in the rear impact mode. Lower-neck loads and lower-neck-injury criteria (LN_{ij}) were obtained using the load cell data and survival analysis to develop injury-assessment-risk values and curves for both dummies. The LN_{ij} criteria were determined for both dummies using the intercept value corresponding to the 90% probability level for the forces and moments.

Results: The lognormal and Weibull distributions were the optimal distributions for the Hybrid III and THOR devices. At the 50% risk level, the mean LN_{ij} of 1.1 and NCIS was 0.77 for the Hybrid III, and 1.5 NCIS was 0.30 for the THOR device. The quality indices were in the fair range and good range for the 2 dummies, respectively, at this risk level.

Conclusions: The lower neck based LN_{ij} injury assessment risk values and curves, IARCs and IARVs, serve as the first dataset for injury assessments, and the THOR may be a better test device for assessing injures in rear impact environments.

INTRODUCTION

Injury risk curves from human cadaver experiments are available for rear impacts and this includes force, moment and lower-neck-injury criteria variables (Yoganandan et al., 2017). To advance human safety and improve vehicle performance, it is important to use human cadaver outcomes and develop injury criteria for anthropomorphic test devices, i.e., injury assessment risk values and curves (IARVs and IARCs). The frontal impact dummy Hybrid III also is used for rear impact crashworthiness in automotive, military, and astronaut environments. The Test Device for Human Occupant Restraint, termed the THOR, also can be used for this purpose. The objectives of the study are to derive lower neck injury probability curves under rear impact loading for intact and isolated head-neck models from both dummies and develop IARCs and IARVs.

METHODS

Twelve whole-body rear impact sled tests were conducted with the THOR and Hybrid III dummies. The dummies were positioned on a rigid seat attached to the top of an acceleration sled. They were positioned with the head parallel to the ground, torso against the seat back, and legs stretched such that there was no axial rotation. Head restraint was not used. The applied rear impact acceleration pulse matched previous in-house PMHS tests (Yoganandan et al., 2000). The 6-axis lower neck load cell was used in both dummies for gathering neck loads and moments. A linear accelerometer was mounted to the sled. Fifteen isolated rear impact sled tests were conducted using the 2 dummies. The lower neck load cell was mounted to the top of a sled with the head parallel to the ground, and this also paralleled in-house human cadaver tests (Yoganandan et al., 2017). The lower neck shear force and extension bending moments were obtained from the inferior load cell. The interaction-based force and moment lower neck injury criteria LN_{ij} were obtained (FMVSS-208, 2001; Kleinberger et al., 1998). Its formulation is given by the F force and its critical intercept F_{crit}, and moment M and its critical intercept M_{crit}. The critical values were obtained from the force and moment risk curves corresponding to 90% mean data.

$$LN_{ij} = \frac{F}{F_{crit}} + \frac{M}{M_{crit}}$$

Because matched-pair tests were conducted, the IARCs were developed based using the combination of injury outcomes and dummy-recorded loads. They were derived using the peak shear force and peak extension moment using the following censoring scheme. If the cadaver specimen was subjected to 1 impact test, the injury metric was considered as right censored if the outcome was associated with no injury and was considered as left censored if injury was the outcome. If repeated tests were conducted on the same specimen, data were considered as interval censored using the highest noninjury test and the test that resulted in injury. The Weibull, lognormal, and loglogistic distributions were considered for developing the IARCs. The plus and minus 95% confidence intervals were computed using the delta method. The normalized confidence interval size (NCIS) was calculated at discrete probability levels: 5%, 10%, 20%, 50%, and 90%. The index was defined as good, fair, marginal, and acceptable based on NCIS magnitudes of NCIS < 0.5, 0.5 ≤ NCIS < 1.0, 1.0 ≤ NCIS ≤1.5, and NCIS > 1.5. This has been used in other studies.

RESULTS

For the Hybrid III dummy, the lognormal was the optimal distribution for forces and moments. The critical intercepts at the 90% risk for the force and moment were 565 N and 117 Nm, respectively. For the THOR dummy, the lognormal was the optimal distribution for the forces and Weibull distribution for the moments. The critical intercepts at 90% risk for the force and moment were 342 N and 85 Nm, respectively. The LN_{ij} criteria were determined for both dummies using the intercept value corresponding to the 90% probability level for the forces and moments. The lognormal distribution again was found to be the optimal distribution for the Hybrid III dummy. The mean LN_{ij} of 1.1 was associated with 50% injury probability, and NCIS was 0.77. The quality index was in the fair range. The IARCs and NCIS bar charts are shown in Figure 1 (left and right plots). The Weibull distribution was the optimal distribution for the THOR dummy. The mean LN_{ij} of 1.5 was associated with 50% injury probability, and NCIS was 0.30. The quality index was in the good range. For the two dummies, the IARCs and NCIS charts are shown in Figures 1 and 2.

DISCUSSION

To meet the objectives of the study, matched-pair tests were conducted with the Hybrid III and THOR dummies. They paralleled previously conducted human cadaver tests: dummies tested as full surrogates and isolated head-neck models. The average of 3 dummy tests for each device was used for the development of IARCs, a norm followed in the automotive literatures. The use of the survival analysis is in line with the most recent processes for developing IRCs and IARCs, as it accounts for censoring and produces zero risk at null stimulus, a limitation of the previously published binary regression models (Yoganandan et al., 2016). The critical intercept based on the IARCs from the forces and moments are based on the accepted methodology used in the human cadaver IRC developments. Thus, the experiments, development of risk curves, and derivation of the interaction criteria are according to accepted biomechanical and statistical processes. The IARCs and IARVs from this analysis is robust, while acknowledging that the PMHS size is low. Although additional experiments are needed, the present results serve as a first step in the delineation of lower neck injury criteria. Across all risk levels, the examination of the quality of the IARCs showed that the Hybrid III dummy responses are in the fair to acceptable range, while the THOR dummy responses were better, i.e., in the good to fair range. This implies that the THOR dummy may be a better test device for assessing injures in crash environments. This is not a surprising finding when one acknowledges that the Hybrid III was developed in the 1970s, while the THOR is based on more recent biomechanical studies. Further, the THOR dummy has undergone several modifications in the neck construction. The materials and design of the neck of the 2 dummies are different. At the level of rear impact severities considered herein, the findings from this study suggest that the THOR dummy is an improved physical surrogate over the Hybrid III for crashworthiness studies, and the present IARCs and IARVs for both dummies serve as the first dataset for injury assessments (PMHS sustained mainly ligament and soft tissue injuries, AIS <2) under this mode of loading.

ACKNOWLEDGEMENTS

This work was supported by the Office of the Assistant Secretary of Defense for Health Affairs, through the Broad Agency Announcement under Award No. W81XWH-16-1-0010, and the Department of Veterans Affairs Medical Research. The Opinions, interpretations, conclusions, and recommendations are those of the authors and are not necessarily endorsed by the Department of Defense or other sponsors

REFERENCES

FMVSS-208, 2001. 49 Code of Federal Regulations. US Government Printing Office, Washington, DC.

Kleinberger, M., Sun, E., Eppinger, R., Kuppa, S., Saul, R., 1998. Development of improved injury criteria for the assessment of advanced automotive restraint systems. NHTSA, Washington, DC, p. 115 pp.

Yoganandan, N., Banerjee, A., Hsu, F.C., Bass, C.R., Voo, L., Pintar, F.A., Gayzik, F.S., 2016. Deriving injury risk curves using survival analysis from biomechanical experiments. J Biomech 49, 3260-3267.

Yoganandan, N., Pintar, F.A., Banerjee, A., 2017. Load-Based Lower Neck Injury Criteria for Females from Rear Impact from Cadaver Experiments. Ann Biomed Eng 45, 1194-1203.

Yoganandan, N., Pintar, F.A., Stemper, B.D., Schlick, M.B., Philippens, M., Wismans, J., 2000. Biomechanics of human occupants in simulated rear crashes: documentation of neck injuries and comparison of injury criteria. Stapp Car Crash J 44, 189-204.

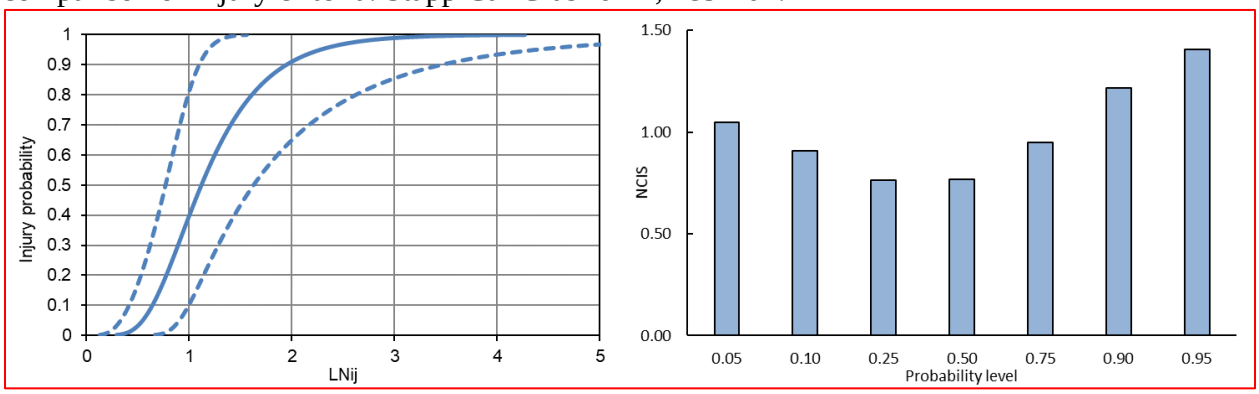

Figure 1: IARCs (left) and NCIS (right) for the Hybrid III dummy.

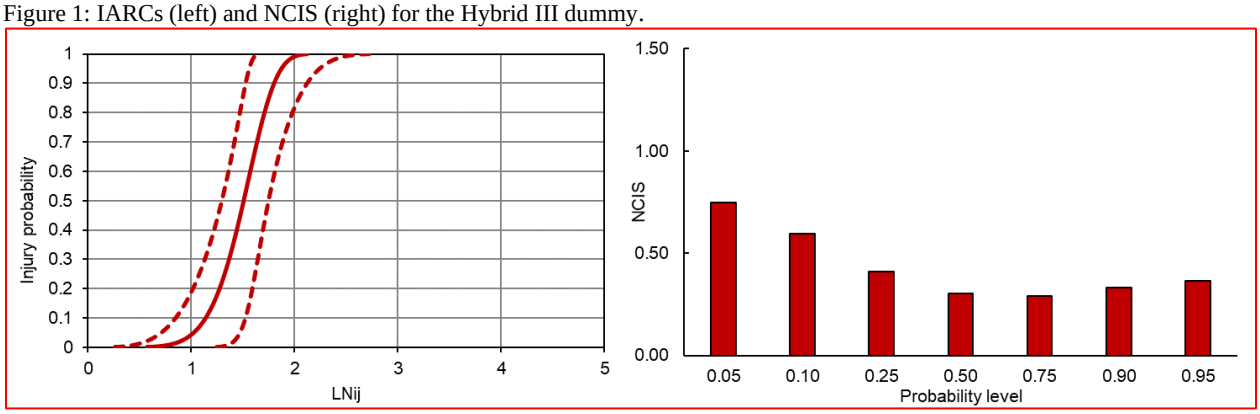

Figure 2: IARCs (left) and NCIS (right) for the THOR dummy.

Thursday, October 15th, 2020, 4:30 PM - 4:40 PM EST

Isometric, Concentric, and Eccentric Neck Strength in the Sagittal and Coronal Planes of Motion for Adult Females

Author: Yadetsie Zaragoza-Rivera, zaragoza-rivera.1@osu.edu
Co-Authors: John Bolte, john.bolte@osumc.edu, Laura Boucher, laura.boucher@osumc.edu

ABSTRACT

Objective: Assess strength in adult females using multiple positions, motions, and contraction types, to better understand strength production of young and non-symptomatic of adult female subjects to help assess and improve the biofidelity of anthropomorphic test devices and human body models.
Methods: Fifteen adult females (25.4 ± 6.3 years) were recruited for this study. Strength measurements were collected for the sagittal and coronal planes during isometric, concentric, and eccentric muscle contractions in neutral and mid-range of motion anatomical positions.
Results: For both planes, subjects were strongest during eccentric muscle contractions and weakest in concentric muscle activations. In the sagittal plane, subjects were stronger in extension for all muscle activation types and anatomical positions. In the coronal plane, there were no side differences in isometric nor concentric strength.
Conclusions: Neck strength of adult females depends on muscle activation type and anatomical positions. Future computational models should account for muscle activation type when quantifying responses of female subjects.

INTRODUCTION

Adult females are more likely to suffer whiplash injuries during vehicle crashes than male occupants (Hoy et al., 2010). The increased vulnerability to severe injuries and mortality of female occupants can be attributed to a lack of female focused safety systems (Yoganandan et al., 2017). A need for the understanding of the unique biomechanical characteristics caused by the physical and physiological dimorphism between males and females are needed. There is a need to better understand the specific strength characteristics of the female cervical spine in a variety of engagements to further assess the biomechanical response of this population. The present study characterizes neck strength in isometric, concentric, and eccentric muscle activations in the sagittal and coronal planes for a variety of anatomical positions in non-symptomatic adult females.

METHODS

This study was reviewed and approved by the Institutional Review Board (IRB) at the Ohio State University, Columbus OH (Project #2016H0300). Fifteen adult females aged 25.4 ± 6.3 years (range: 20–40 years) were recruited for this study. Exclusion criteria were injury to the neck within the last year, neck surgery within their lifetime, excessive kyphosis, allergies to adhesive tape, and head girth ≤ 56 cm. Peak strength (Nm) was defined as the maximum measurement for each muscle contraction at each anatomical position.

Isometric Strength

Strength measurements were recorded using a Biodex Isokinetic Dynamometer (Biodex Medical Systems Inc., Shirley, New York) (Figure 1). The Biodex was fit to each participant such that the fulcrum of the rotation for each test occurred at the palpated C7 protrusion of each subject (Figure 2). Measurements were recorded for neutral anatomical position (0° of axial deviation)

and at mid-range of motion (30° of neck bending) in the sagittal and coronal planes. In the sagittal plane, subjects performed flexion and extension isometric strength measurements (Figure 3a). In the coronal plane, subjects preformed left and right lateral bending (Figure 3b). For each measurement subjects completed three, 5 second isometric contractions, with 5 seconds of rest between repetitions.

Dynamic Strength

Concentric and eccentric strength were evaluated during a dynamic testing protocol, with the Biodex moving at a rate of 30°/s through each motion (Figure 3c, 3d). Concentric strength was measured as peak strength when subjects were engaging toward the same direction as the Biodex was moving. Eccentric strength was the peak strength value when subjects engaged against the motion of the Biodex. Subjects moved through a 60° arc of total motion, and 30° in each direction for flexion-extension and left-right lateral bending. Dynamic strength was stratified per the subjects' effort and anatomical position.

Statistical Analysis

Statistical analyses were performed using JMP 14 (SAS Institute Inc., Cary NC). Descriptive statistics were used to compare overall cohort means and standard deviations (SD). Statistical analyses were conducted at an α-level of 0.05. Student's t-test were performed using Wilcoxon/Kruskal-Wallis statistics.

RESULTS

Isometric Strength

In the sagittal plane, isometric flexion strength significantly varied based on anatomical position. Flexion at mid-range of motion when flexed was significantly greater than at neutral ($p < .0001$) and while extended ($p = 0.043$). Flexion at neutral was significantly greater than when extended. In extension, strength at mid-range when extended was significantly greater than in neutral ($p = 0.002$) and when flexed ($p < .0001$). Subjects were always stronger in extension regardless of neck position. In the coronal plane, isometric strength measurements toward the right side of lateral bending did not significantly vary with location and all right side measurements were within 3 Nm of each other. Isometric strength toward the left side had significant differences based on location, with bending toward the left being stronger than neutral ($p = 0.037$) and bending toward the right ($p = 0.002$). Subjects were always stronger at mid-range of motion when laterally bent to the same side of engagement.

Dynamic Strength

In the sagittal plane, subjects were stronger in the same direction they were flexed regardless of type of concentric or eccentric contraction (Table 1). When comparing flexion and extension, subjects were always stronger in extension for both concentric and eccentric muscle contractions. Subjects were stronger eccentrically regardless of anatomical position. In the coronal plane, there were no significant differences in concentric strength between the sides when subjects were engaging toward the same side they were laterally bent or when they were engaging to the opposite side they were laterally bent. Concentrically, subjects were significantly stronger when pushing toward the side they were laterally flexed. Right eccentric lateral bending was significantly stronger than the left side (Table 2).

DISCUSSION

This study assessed neck strength in isometric, concentric, and eccentric contractions of asymptomatic adult females both for the sagittal and coronal planes. Overall subjects were

always stronger at mid-range of motion and with contraction to the same side they were flexed. In the sagittal plane, subjects were always stronger in extension. This trend in strength production has been reported in literature and it is believed to be related to the increased sized and amount of musculature working in extension compared to flexion (Salo et al., 2006). In the coronal plane, strength did not vary by side in isometric and concentric muscle contractions. However eccentrically, subjects were stronger on the right side. We hypothesized that this difference in strength may be related to subjects' natural side preference, as all subjects self-identified as right handed. While this study has a small sample size, it offers a comprehensive assessment of neck strength in a variety of anatomical positions and muscle contractions for healthy adult females. Strength of adult depend on type of muscle contractions. Subjects were weakest with concentric contractions and strongest in eccentric contractions. These data may help the future development of anthropomorphic test devices and computational models to better assess the kinetic and kinematic responses of female vehicle occupants.

REFERENCES

1. Hoy DG, Protani M, De R, Buchbinder R. The epidemiology of neck pain. *Best Pract Res Clin Rheumatol*. 2010;24(6):783-792. doi:10.1016/j.berh.2011.01.019.
2. Salo PK, Ylinen JJ, Mälkiä EA, Kautiainen H, Häkkinen AH. Isometric strength of the cervical flexor, extensor, and rotator muscles in 220 healthy females aged 20 to 59 years. *J Orthop Sports Phys Ther*. 2006;36(7):495-502. doi:10.2519/jospt.2006.2122.
3. Yoganandan N, Bass CR, Voo L, Pintar FA. Male and Female Cervical Spine Biomechanics and Anatomy: Implication for Scaling Injury Criteria. *J Biomech Eng*. 2017;139(5):1-5. doi:10.1115/1.4036313.

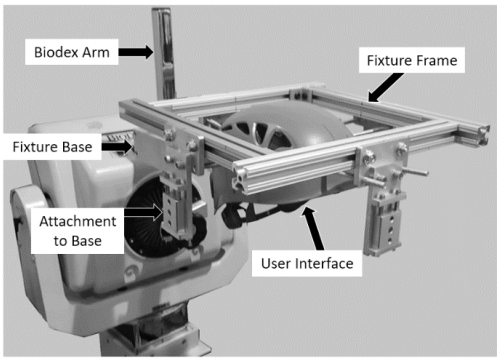

Figure 1. Custom head fixture retrofitted on a Biodex Isokinetic Dynamometer

a) 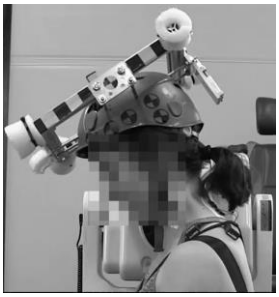 b) 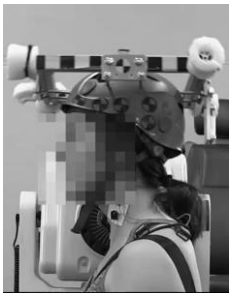 c) 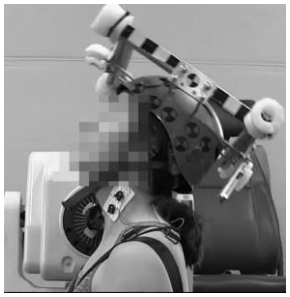

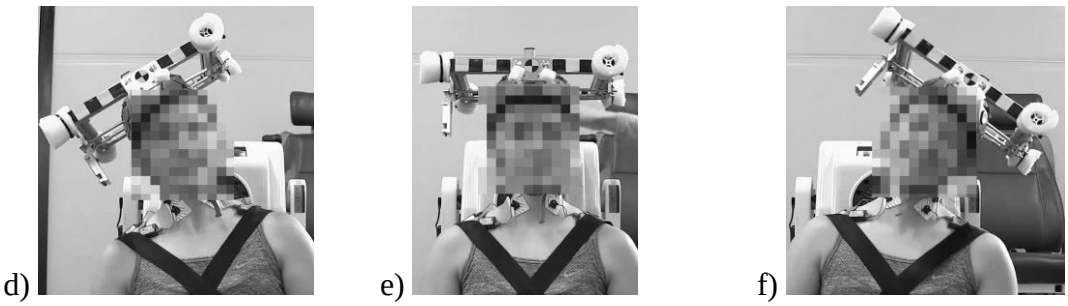

Figure 2. Subject in the testing equipment. Top: Sagittal plane engagement. Bottom: Coronal plane engagement. A-C) Subject in mid-range flexion, neutral, and mid-range extension positions. D-F) Subject in right lateral bending, neutral, and left lateral bending positions.

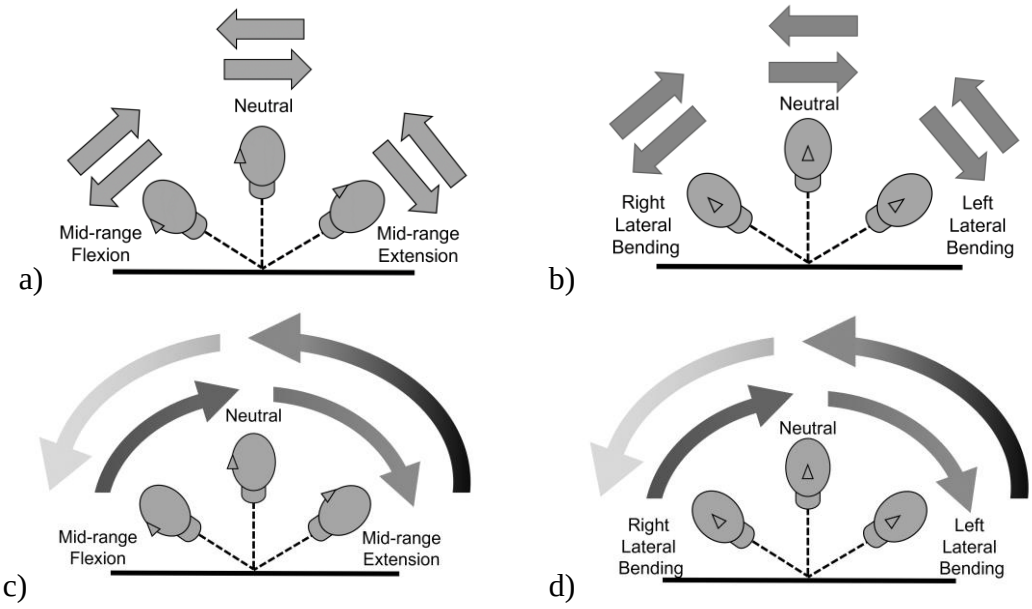

Figure 3. Schematics of the testing setup. Top: Subject's efforts (represented by arrows) during the isometric testing condition at neutral and mid-range of axial deviation. Bottom: Subject's motion (represented by curved arrows) during dynamic testing; where concentric or eccentric engagement was achieved with engagement with or against the motion, respectively. A, C) Sagittal plane engagement. B, D) Coronal plane engagement.

Table 1. Strength by muscle engagement in Nm (SD) for the sagittal plane.

Engagement	**Mid-Range Flexed**		**Neutral**		**Mid-Range Extended**	
Type	Flexion	Extension	Flexion	Extension	Flexion	Extension
Isometric	13.85 (2.53)	15.26 (3.78)	7.75 (1.76)	17.88 (3.93)	4.08 (1.78)	21.77 (3.85)
Concentric	10.33 (2.10)	11.93 (4.13)			2.80 (1.96)	15.94 (4.01)
Eccentric	10.95 (2.98)	15.55 (6.58)			8.24 (2.79)	19.60 (5.78)

Table 2. Strength by muscle engagement in Nm (SD) for the coronal plane.

	Mid-Range Right	**Neutral**	**Mid-Range Left**

Engagement Type	Right	Left	Right	Left	Right	Left
Isometric	15.74 (2.60)	10.67 (4.41)	12.82 (3.06)	12.26 (3.34)	12.12 (3.75)	15.86 (2.49)
Concentric	13.05 (2.93)	8.58 (3.18)			8.95 (3.88)	12.35 (2.21)
Eccentric	14.69 (3.73)	10.97 (4.41)			14.03 (4.26)	13.42 (4.30)

Thursday, October 15th, 2020, 4:40 PM - 4:50 PM EST

Development of Chest Deflection Injury Risk Curve in Oblique Frontal Small Female PMHS Sled Tests

Author: John Humm, jhumm@mcw.edu
Co-Author: Narayan Yoganandan, yoga@mcw.edu

ABSTRACT

Objective: The study's aim is to examine which sternum deflection measure best represents injury in oblique frontal impacts with small female surrogates.
Methods: Data from sixteen PMHS sled tests were used to calculate sternum deflection using displacements in the A-P (x) direction, transverse (xy) plane, sagittal (xz) plane, and triplanar (xyz). Peak deflections were the response variable and were combined with injury outcomes to generate injury risk curves (IRCs) using parametric statistical survival modeling. The IRC with the lowest Brier Score Metric was considered the best deflection measure representing injury.
Results: The triplanar (xyz) deflection metric was the best indicator of injury. At the 10 and 50% probability levels, the magnitudes of this metric were 33 mm and 55 mm, respectively. The quality of the risk curve was fair for 10% and good for 50%, based on the ISO recommendations.
Conclusions: The current study reports on the injury risk to small females in an upright seated position in oblique frontal impacts. The triplanar and transverse plane deflection metrics were similar for this posture; however, occupants in reclined configurations may demonstrate a different response, and further investigations are necessary.

INTRODUCTION

Automotive safety research has used laboratory studies with biological surrogates (e.g., post mortem human subjects, PMHS) to replicate field-identified injuries and derive injury criteria. Response corridors and injury criteria from PMHS laboratory tests guide the development and design of Anthropomorphic Test Devices (ATDs) and computational models. These efforts are used to assess vehicle crashworthiness and promulgate standards to improve automotive safety. For the thorax, rib fractures are the most common injury in automobile environments. Peak chest deflection has been associated with thoracic injury. PMHS sled tests mimicking standard automotive restraints and geometries (Shaw et al., 2009) were used to validate the 50% male Test Device for Human Occupant Restraint (THOR-50M) ATD. Both the 50M and 05F (small size female) devices can record three-dimensional chest deflections at multiple locations. While these devices are intended to be used for pure and oblique frontal crashworthiness studies, an evaluation of the effectiveness of the multi-axis deflections has not been made with specific reference to small size female occupants in oblique impacts. The objective of the current study is to examine combined thoracic deflections metrics from previously conducted small female

PMHS sled tests using parametric statistical survival modeling (PSSM) and determine the deflection metric that best represents injury.

METHODS

Sixteen PMHS representative of the small-female population were subjected to oblique frontal sled tests (Humm et al., 2018). Ten specimens were subjected to a 30 km/h pulse and the remaining six to a 15 km/h pulse. Injuries were classified according to the Abbreviated Injury Scale (2015 version). Retroreflective targets were fixed to the dorsal spine at T8, ventral thorax at the sternum, and seat. A 28-camera motion-capture system (Vicon Motion Systems Ltd, UK) was used to record the three-dimensional kinematics of the targets. These data were combined with pre-test CT scans of the PMHS and coordinate-measuring machine data of the buck to determine the occupant's kinematics. Thoracic deflections were found by calculating the position of the sternum origin with respect to the T8 local coordinate system at each time-step. Four types of kinematic metrics representing thoracic deflection were defined— x-only (single-axis representing the anteroposterior component), x-y and x-z (representing the transverse and sagittal planes), and x-y-z (representing all three planes)— and were calculated as the difference of the square root of the sum of the squares of the sternum from its initial location. AIS 2+ Injury Risk Curves (IRCs) were developed by considering PMHS outcomes of AIS 2 or greater as injured while PMHS outcomes with AIS of less than or equal to 1 were considered non-injured. All four peak deflections were used as response variables, and injury data were treated as uncensored, while the non-injury data were right-censored. PSSM was performed using updated techniques from the ISO/TC22/SC12/WG6 working group of the International Organization for Standardization (ISO) recommendations (Yoganandan et al., 2016). The Weibull, log-logistic, and lognormal distributions were used in the analysis. The Brier Score Metric (BSM) was calculated for each response variable, and the optimum distribution was selected based on the lowest Akaike Information Criterion, AIC. The deflection that produced the lowest BSM was considered to the best metric that described the sternum deflection response to oblique frontal impacts.

RESULTS

Specimen demographics for age, mass, and stature were 74.4 ± 11.7 years, 46.8 ± 6.8 kg, and 1.57 ± .06 m. Nine specimens were in the noninjury, and seven were in the injury group. For the x, x-y, x-z, and x-y-z deflections, Weibull distributions were used, and the BSMs were 5.40, 5.18, 5.29, and 5.17, respectively. The difference between the average peak deflection compared to the x-y-z of the x, x-y, and x-z was 8.6, 3.8, and 4.5%. Figure 1 shows a lateral view of the T8 and sternum trajectories and anatomic orientation with respect to the seat. Figure 2 shows the calculated IRC for x-y-z (multi-axis) sternum deflection. The 50% risk levels were 49.4, 52.5, 51.9, and 54.9 mm for the x, x-y, x-z, and x-y-z, respectively.

DISCUSSION

The objective of the current study was to evaluate chest deflections metrics for small-female PMHS in oblique frontal sled tests. Chest deflection was selected as the injury metric as it reliably characterizes chest injuries in frontal and oblique impacts and is measurable with THOR-05F. The present results are applicable to the driver occupant kinematics as the specimens were seated in a standard driving position. From a statistical perspective, the triplanar deflection IRC was equivalent to the transverse-plane deflection, which was not unexpected

given the oblique loading vector to the occupant. More notably, it is anticipated that occupant seating postures will change (e.g., reclined postures and/or obliquely mounted seats) as the industry progresses to higher levels of autonomous vehicles. The kinematics of the upright seated occupant shown in Figure 1 demonstrate the forward and vertical excursion of the spine as it straightens and rotates over the fixed pelvis while the sternum's motion is limited by the shoulder belt. Alternate seating configurations may change the thoracic response of the occupant, and experiments with PMHS in these scenarios are currently being explored by the authors. The methods of the current study will be used to examine chest deflection metrics in these conditions. Because of the small sample size, the IRCs should be considered as preliminary tolerance data for females. Additional tests are needed to increase the robustness of the IRC and examine factors such as age and body mass index on injuries. Uncertainties in the motion-capture data are a source of error and are approximately 1-2 mm for this rate of loading and capture volume. The current results indicate that the peak sternum x-y-z (triplanar) deflection is the optimal metric that best describes the underlying response to chest injuries at the AIS 2+ level to small females from oblique frontal impacts.

ACKNOWLEDGEMENTS

The authors thank the AAAM for supporting this research through the AAAM Scholar's Program, the National Highway Traffic Safety Administration, and the Office of the Assistant Secretary of Defense for Health Affairs, through the Broad Agency Announcement under Award No. W81XWH-16-1-0010. This study was was also supported by the Department of Veterans Affairs Medical Research. Opinions, interpretations, conclusions, and recommendations are those of the authors and are not necessarily endorsed by the Department of Defense or other sponsors.

REFERENCES

Humm JR, Yoganandan N, Driesslein KG, Pintar FA. 2018. Three-dimensional kinematic corridors of the head, spine, and pelvis for small female driver seat occupants in near- and far-side oblique frontal impacts. Traffic Inj Prev 19:S64-S69.

Shaw G, Parent D, Purtsezov S, Lessley D, Crandall J, Kent R, Guillemot H, Ridella SA, Takhounts E, Martin P. 2009. Impact response of restrained PMHS in frontal sled tests: skeletal deformation patterns under seat belt loading. Stapp Car Crash J 53:1-48.

Yoganandan N, Banerjee A, Hsu FC, Bass CR, Voo L, Pintar FA, Gayzik FS. 2016. Deriving injury risk curves using survival analysis from biomechanical experiments. J Biomech 49:3260-3267.

TABLES AND FIGURES

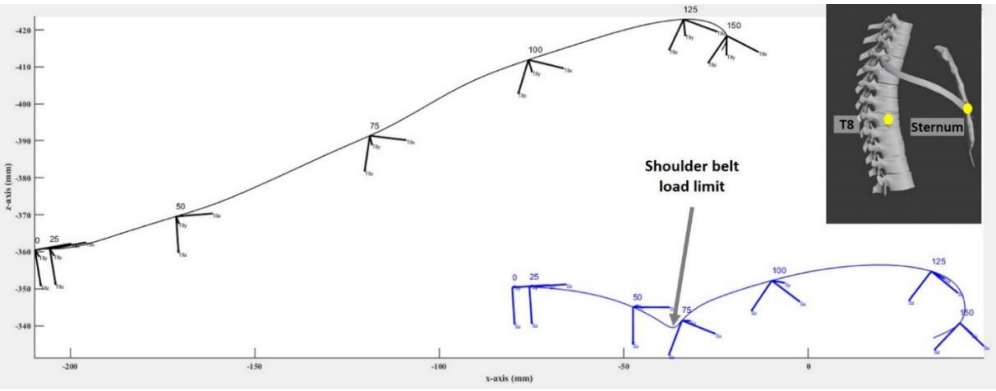

Figure 1: Right side view of T8 (black) and sternum (blue) trajectories with respect to the seat for a representative high-speed PMHS sled test.

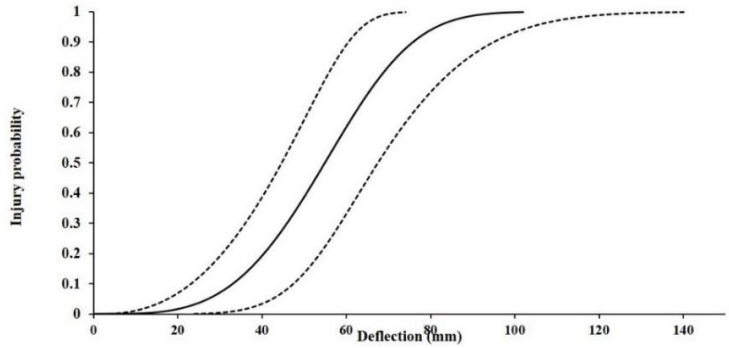

Figure 2: AIS 2+ Injury Risk Curve for peak x-y-z (triplanar) sternum deflection.

Thursday, October 15th, 2020, 4:50 PM - 5:00 PM EST
Intervertebral Foramen Narrowing During Vertical Dynamic Loading
Author: Dennis Maiman, dmaiman@mcw.edu
Co-Authors: William Curry, wcurry@mcw.edu, Narayan Yoganandan, yoga@mcw.edu, Frank Pintar, fpintar@mcw.edu

ABSTRACT
Objective: The goal of the present study was to examine the effect of vertebral body fracture on the InterVertebral Foraminal IVF parameters with an input acceleration to the seat bottom in the inferior-to-superior direction. **Methods:** A series of 43 isolated lumbar spines underwent vertical dynamic loading using the vertical accelerative device to determine the influence of inferior to superior loading through the lumbar spine on the intervertebral foramen (IVF) geometries. Existence of foraminal stenosis was quantified using pre- and post-test computed tomography (CT) images. Foraminal height (IVF_Ht) and posterior disc height (PD_Ht) were the key IVF parameters. **Results**: There was a significant ($p<0.05$) decrease in the post-test IVF measurements compared to the pre-test measurements. Furthermore, 30% of the total 49 AIS 2 cases and 70% of the total 21 AIS 3 cases had IVF values below the literature reported thresholds for IVF_Ht of < 15 mm and PD_Ht of < 4mm, indicating likely occurrence of foraminal stenosis. **Conclusions**: These results underscore the need to assess foraminal geometry in compression fractures of the lumbar spine from vertical dynamic loading.

INTRODUCTION
Axial loading of the spinal column through the pelvis has been implicated in 86% of all spinal fractures, from those wounded in military underbody blast (UBB) events without rollover, as well as numerous less-severe civilian motor vehicle crashes. These are typically due to vertical compression of the spine, primarily concentrated in the lumbar region [29% of all UBB associated injuries (Danelson et al., 2015)]. Thoracolumbar spine injuries have also been identified in automotive crashes to restrained occupants in frontal impacts (Pintar et al., 2012). Injury to this region is of particular concern since the spinal cord, associated nerve roots, and the cauda equina can also be injured, resulting in a broad range of clinical outcomes. Even in the

absence of severe vertebral body injury, back and radicular pain may persist (Weninger et al., 2009). The goal of the present study was to examine the effect of vertebral body fracture on the IVF geometrical parameters with an input acceleration to the seat bottom in the inferior-to-superior direction.

METHODS

Forty-three isolated thoracolumbar spinal columns were tested on a custom vertical accelerative device. Specimen preparation and instrumentation has been described elsewhere (Yoganandan et al., 2020). Briefly, whole lumbar spinal columns were excised from 43 PMHS. The specimens were fixed at the ends, aligned in a consistent seated posture, load cells were attached to the proximal and distal ends of the fixation, and the vertical impact loading was applied using the custom. Pretest x-rays and computed tomography (CT) scans, prepositioned x-rays, and posttest x-rays, CT scans, and dissection data were used to identify injuries. The impact velocities ranged from 0.3 to 12.3 m/s. All scans were performed using an axial CT scanner with a slice thickness of 0.625 mm and a plane resolution of 512 x 512 pixels. The scans were obtained in DICOM format and loaded onto OSIRIX (Pixmeo, Inc., Geneva). Foraminal height (IVF Ht) and posterior disc height (PD Ht) were measured (Ohba et al., 2015). Fractures were graded for presumed clinical significance using AIS 2015 scoring by the senior author (AIS, 2015). The entire course of the IVF was examined by resampling the acquired CT scans in the sagittal plane using the pedicle as a guide (Figure 1).

RESULTS

Results of the tests showed 40 injuries (out of an original set of 43), including single and multiple level fracture sets. This study produced 49 AIS 2 and 21 AIS 3 fracture cases (Table 1). The foraminal and posterior disc height for each of these cases were then calculated, and they showed a ($p<0.05$) decrease in post-test IVF measurements compared to the pre-test. Previous radiculopathy studies[4-8] have demonstrated that significant nerve root compression is commonly associated with a foraminal height of 15 mm or less and a posterior disc height of 4 mm or less and these values might be indicator of lumbar foraminal stenosis. In the current study, 15 of the 49 AIS 2 and 14 of the 21 AIS 3 cases had post-test IVF measurements below the reported thresholds. Specimen age and bone mineral density between those with IVF values < thresholds vs above the thresholds are given; they were not different (Table 1). Furthermore, all the cases with foraminal height below the threshold also had posterior disc values below the threshold even though the converse was not true. Both separated and combined IVF measurements are provided in Table 2.

DISCUSSION

Although only two parameters were considered, this preliminary study is first of its kind to investigate the influence of vertical loading through the spine on IVF parameters. This study provides a comparison between the vertebral body fracture scored using AIS coding, which is based on anatomy of the vertebral body and IVF measurements, indicative of likely occurrence of nerve root compromise, often resulting in motor weakness, sensory loss, or radicular pain.

The presence of foraminal narrowing, especially if chronic, is often not associated with radiculopathy. The cited authors followed asymptomatic patients with degenerative changes in the spine for a decade; in the absence of an acute event, such as a car crash, 15% reported axial

pain but no evidence of neurologic changes, even with severe stenosis (Gore, 2001; Gore et al., 1986; Hasegawa et al., 2011; Hasegawa et al., 1995; Rao et al., 2016).. Chung et al. reported on a series of patients suffering onset of radiculopathy following osteoporotic fractures (Chung et al., 2002). They noted that the majority had preexisting, asymptomatic foraminal stenosis prior to the fracture. Restoration of pre-morbid geometry resulted in clinical improvement. Kim et al. made similar observations, adding that most fractures associated with radiculopathy were at the inferior vertebral body (Kim et al., 2015). Presumably, slow progression of foraminal narrowing is tolerated due to the viscoelastic nature of nervous tissue; an acute change may well exceed that threshold (Kuijper et al., 2011; Lipetz, 2002). As the IVF measurements are small, specimen handling time of imaging are critical. Care was taken to ensure that the protocols for handing and analysis remained the same for all PMHS.

As expected, the majority of AIS 3 cases had an IVF measurement below the literature reported threshold, accounting for 70% of the total. However, it was surprising to find that 30% of the AIS 2 cases also had an IVF measurement below the critical values, indicating a potential occurrence of nerve root compromise even in minor fracture cases. In the future, additional parameters such as anterior/mid-point disc heights, superior/middle/inferior foraminal widths, posterior bulging of intervertebral disc, and width of posterior vertebral margin should be considered. Additionally, this study suggests the need to look at IVF parameters more closely for patients with even minor fractures.

ACKNOWLEDGEMENTS

The data used in this study originated from work conducted under the support of contract #N00024-13-D-6400, sponsored by the U.S. Army Research Lab in support of the WIAMan Program. This work was supported by the Office of the Assistant Secretary of Defense for Health Affairs, through the Broad Agency Announcement under Award No. W81XWH-16-1-0010, and the Department of Veterans Affairs Medical Research. The Opinions, interpretations, conclusions, and recommendations are those of the authors and are not necessarily endorsed by the Department of Defense or other sponsors

REFERENCES

AIS. 2015. The Abbreviated Injury Scale. In: AAAM, editor. Arlington Heights, IL: AAAM

Chung SK, Lee SH, Kim DY, Lee HY. 2002. Treatment of lower lumbar radiculopathy caused by osteoporotic compression fracture: the role of vertebroplasty. J Spinal Disord Tech 15:461-468.

Danelson KA, Kemper AR, Mason MJ, Tegtmeyer M, Swiatkowski SA, Bolte JHt, Hardy WN. 2015. Comparison of ATD to PMHS Response in the Under-Body Blast Environment. Stapp Car Crash J 59:445-520.

Gore DR. 2001. Roentgenographic findings in the cervical spine in asymptomatic persons: a ten-year follow-up. Spine (Phila Pa 1976) 26:2463-2466.

Gore DR, Sepic SB, Gardner GM. 1986. Roentgenographic findings of the cervical spine in asymptomatic people. Spine (Phila Pa 1976) 11:521-524.

Hasegawa K, Shimoda H, Kitahara K, Sasaki K, Homma T. 2011. What are the reliable radiological indicators of lumbar segmental instability? J Bone Joint Surg Br 93:650-657.

Hasegawa T, An HS, Haughton VM, Nowicki BH. 1995. Lumbar foraminal stenosis: critical heights of the intervertebral discs and foramina. A cryomicrotome study in cadavera. J Bone Joint Surg Am 77:32-38.

Kim DE, Kim HS, Kim SW, Kim HS. 2015. Clinical analysis of acute radiculopathy after osteoporotic lumbar compression fracture. J Korean Neurosurg Soc 57:32-35.
Kuijper B, Tans JT, van der Kallen BF, Nollet F, Lycklama ANGJ, de Visser M. 2011. Root compression on MRI compared with clinical findings in patients with recent onset cervical radiculopathy. J Neurol Neurosurg Psychiatry 82:561-563.
Lipetz JS. 2002. Pathophysiology of inflammatory, degenerative, and compressive radiculopathies. Phys Med Rehabil Clin N Am 13:439-449.
Ohba T, Ebata S, Fujita K, Sato H, Devin CJ, Haro H. 2015. Characterization of symptomatic lumbar foraminal stenosis by conventional imaging. Eur Spine J 24:2269-2275.
Pintar FA, Yoganandan N, Maiman DJ, Scarboro M, Rudd RW. 2012. Thoracolumbar spine fractures in frontal impact crashes. Ann Adv Automot Med 56:277-283.
Rao RD, Gore DR, Tang SJ, Rebholz BJ, Yoganandan N, Wang M. 2016. Radiographic Changes in the Cervical Spine Following Anterior Arthrodesis: A Long-Term Analysis of 166 Patients. J Bone Joint Surg Am 98:1606-1613.
Weninger P, Schultz A, Hertz H. 2009. Conservative management of thoracolumbar and lumbar spine compression and burst fractures: functional and radiographic outcomes in 136 cases treated by closed reduction and casting. Arch Orthop Trauma Surg 129:207-219.
Yoganandan N, DeVogel N, Moore J, Pintar F, Banerjee A, Zhang J. 2020. Human Lumbar Spine Responses from Vertical Loading: Ranking of Forces Via Brier Score Metrics and Injury Risk Curves. Ann Biomed Eng 48:79-91.

TABLES AND FIGURES

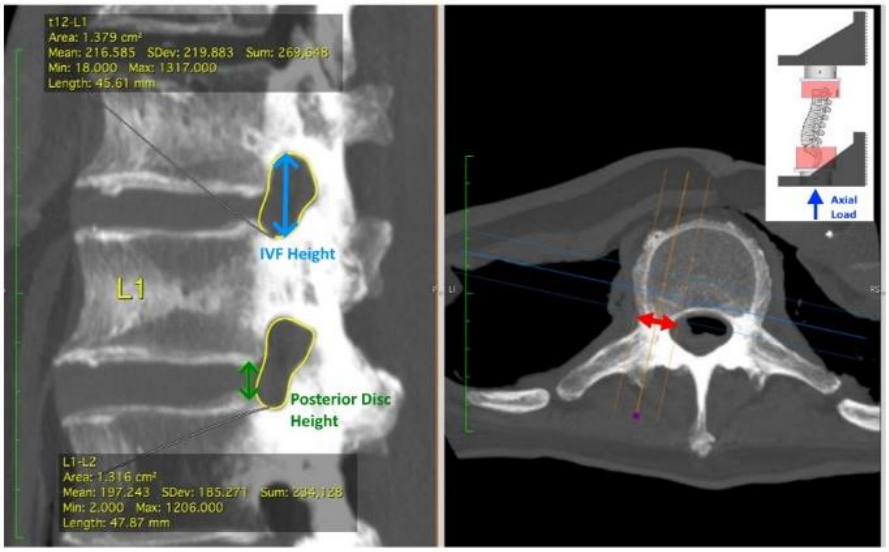

Figure 1. Alignment of the scans along the midline of the pedicle on the axial and sagittal planes, respectively. Foramen and posterior disc height are also shown. The inset image shows the actual test setup.

Table 2: Specimen characteristics that differed between those with IVF values < thresholds vs above the thresholds.

Variable		Values greater than threshold					
		AIS 2			AIS 3		
		IVF	PDH	IVF+PDH	IVF	PDH	IVF+PDH
Age (years)	Mean	66	67	66	NA	NA	NA
	Std	8	11	8	NA	NA	NA
BMD (mg/cc)	Mean	138	121	138	NA	NA	NA
	Std	44	39	44	NA	NA	NA
		Values less than threshold					
Age (years)	Mean	67	66	67	61	61	61
	Std	9	8	9	13	13	13
BMD (mg/cc)	Mean	123	132	123	155	155	155
	Std	23	35	23	58	58	58

Table 2: Summary of data

AIS	Total cases	# IVF-Ht < 15 mm	# Post-Disc < 4 mm	# IVF-Ht < 15 mm + Post-disc < 4mm
2	49	16 (0.33)	24 (0.49)	15 (0.31)
3	21	15 (0.71)	14 (0.67)	14 (0.67)

Friday, October 16th, 2020
10:00 AM - 11:35 AM: Real World & Database Analysis

Friday, October 16th, 2020, 10:45 AM - 10:55 AM EST
Survivability of a Tesla Collision into a Non-operational Crash Attenuator in Mountain View, CA
Author: Thomas Barth, thomas.barth@ntsb.gov
Co-Authors: Mary Pat McKay, mary.mckay@ntsb.gov, Ryan Smith, ryan.smith@ntsb.gov

ABSTRACT
Objective: On March 23rd, 2018 a Tesla Model X driver was killed in Mountain View, CA after colliding with a previously collapsed crash attenuator at a speed of 31.7 m/s (70.8 mph). The attenuator, which must be repaired following a collision, had been struck 11 days prior by a 2010 Toyota Prius at a minimum speed of 33.9 m/s (75.8 mph). The Toyota driver survived. The maintenance of traffic safety hardware and benefit of the crash attenuator are evaluated.
Methods: Public information from an NTSB investigation is used to evaluate crash impact severity. Vehicle crash data from Event Data Recorders (EDRs) are compared with test data for the SCI Smart Cushion 100GM crash attenuator. An idealized triangular crash pulse is used to estimate longitudinal peak impact acceleration, and longitudinal impact energy is calculated. The medical outcomes for drivers are considered.
Results: The California Department of Transportation (Caltrans) maintenance and repair program for safety critical traffic safety hardware was found to be ineffective. The Tesla collision into the

non-functional attenuator was estimated have roughly 3 times the impact force to the passenger compartment as it would have been if striking a functional attenuator.
Conclusions: The Tesla driver could have survived the collision had the crash attenuator been functional. Roadway management and timely maintenance of safety critical traffic hardware are necessary to ensure safety.

INTRODUCTION

Modern technology is changing the motor vehicle environment. Partially automated driving systems can avoid collisions, but driver overreliance and system limitations can also lead to high speed crashes. An NTSB investigation was conducted of such an event, when a 2017 Tesla Model X collided head-on into a crash attenuator in Mountain View, California, killing the driver. At the time of the event, the Tesla driver was relying on the Tesla Autopilot lane-keeping assist system while traveling south on US Highway 101. The Tesla Autopilot system acquired the incorrect lane line of a left-exit ramp. The Tesla entered the gore area and stuck a crash attenuator, which is installed at a location with frequent high-speed frontal collisions. The attenuator was not functional due to a previous collision from a 2010 Toyota Prius. The Toyota impacted the attenuator, collapsing and damaging the telescopic energy absorption system. The Toyota driver was treated at the hospital and survived; he suffered a 5 mm intimal tear of the aorta and an open fracture of one finger on his left hand. The Tesla and Toyota drivers were both wearing lap/shoulder restraints, and the airbags in both vehicles deployed. The road safety management of repairing the attenuator, the performance of the attenuator, and the medical outcomes for the drivers are considered.

METHODS

The NTSB investigation into the March 23, 2018 Tesla crash was reviewed as it pertained to the State's communication and maintenance systems regarding highway traffic safety hardware. Longitudinal crash forces and crash energies for the Tesla and Toyota were estimated and compared by utilizing previous test data for the crash attenuator and crash data from the Tesla and Toyota EDRs. Overall survivability was considered using medical records for the Tesla and Toyota drivers. Performance results of the SCI Smart Cushion 100GM crash attenuator were selected from crash tests conducted by KARCO Engineering in 2015 and 2016 with similar vehicle masses and longitudinal velocity changes. Peak longitudinal accelerations during attenuator interaction were calculated based on idealized triangular crash pulse shapes using velocity change and duration data. Note that the EDRs also provided pre-impact velocity, and which the Toyota EDR measurement limit was 33.9 m/s (75.8 mph). Peak accelerations for the attenuator tests were calculated in a similar manner, using the reported impact speed and impact duration test results. Crash energies for the triangular pulses were also calculated. The Tesla impact was compared to a 2009 Dodge Ram 1500 pickup crash test, and the Toyota impact was compared with a 2010 Chevrolet Malibu crash test. The attenuator stroking distance (displacement) was cited in the KARCO Engineering tests, and this was used to determine the proportion of energy attenuated per meter of displacement. This energy/displacement ratio was used to estimate attenuator benefit for vehicles of similar mass, in order to account for the attenuator non-linear response. The Dodge test was used to estimate the expected displacement of the Tesla, and the Chevrolet test was used for the Toyota.

Limitations include variations in vehicles and impact conditions. Lateral forces and velocity changes were assumed to be small relative to the longitudinal components of the attenuator impact. The general survivability assessment was based on magnitude of force and energy absorbed by the passenger compartment and did not assess detailed injury mechanisms. The medical outcomes of the drivers were compared with the severity of the crashes and estimated potential benefit of the crash attenuator.

Equations: The following equations were used to calculate the peak acceleration and impact energy.

(1) Peak Acceleration (G): $Gpeak = 0.5\Delta v/tg$; where Δv is change in velocity in meters per second, t is duration of the impact in seconds, and g is the acceleration of gravity in meters per second squared.

(2) Impact Energy (Joules): $I.E. = 0.5mv^2$; where m is the vehicle mass in kilograms, v is the velocity in meters per second.

RESULTS

Traffic Safety Hardware Maintenance

The NTSB investigation revealed deficiencies in communication and maintenance of traffic safety hardware. After the Toyota collision, the California Highway Patrol (CHP) failed to notify Caltrans of the attenuator damage, as required by California interagency policy. A routine Caltrans patrol discovered the damaged attenuator 8 days after the Toyota crash, but difficulty locating replacement hardware, staffing shortages, and other work priorities reportedly delayed the repair. The attenuator at this location was found to require more frequent repair than others in the district. Historical records revealed other instances of repair delays, including an instance in 2017, in which this attenuator remained unrepaired for more than 2 months. Caltrans considers attenuators of this type to be first-level priority traffic safety devices, requiring repair within 1 week. Caltrans policy also requires actions if delays occur. A previous NTSB investigation from 2016 found similar problems and had issued recommendations to address the issues. The NTSB concluded that the Caltrans maintenance and repair program was ineffective and recommended that the California State Transportation Agency (parent entity to Caltrans) develop and implement a corrective action plan that guarantees timely repair of traffic safety hardware and includes performance measures to track state agency compliance with repair timelines. Several corrective actions have been implemented, as described in the NTSB report.

Crash Attenuator Performance

The attenuator uses a hydraulic cylinder and cable assembly which collapses in a telescoping manner, decelerating the vehicle as it moves through its stroke. The SCI 100 GM width is 0.601 m wide at the front and 0.808 m at the rear, 0.847 m tall, and 6.550 m long. The maximum stroke and energy capability were not found in literature, however, the KARCO Engineering crash test report includes results with over 5 meters displacement for impact energy exceeding 800 kJ. Test P35022-01 was a frontal collision into the attenuator with a 2009 Dodge Ram 1500 pickup with a mass of 2,270 kg at a speed of 27.09 m/s (60.7 mph); it had 5.2 meters of displacement and impact pulse duration of 0.288 seconds. Test P36142-01 was a frontal collision into the attenuator with a 2010 Chevrolet Malibu with a mass of 1,497 kg and speed of 27.14 m/s (60.6 mph); it had 4.8 meters of attenuator displacement and a pulse duration of 0.300 seconds. The tests resulted in negligible exit velocities and lateral occupant compartment velocities of less than 1% and lateral occupant compartment accelerations of less than 15% of the longitudinal values.

Tesla and Toyota Crash Pulses

EDR data provides longitudinal impact velocity changes and impact pulse durations for the Tesla and Toyota collisions. Although the pre-impact speeds were 31.65 m/s (70.8 mph) and a minimum of 33.89 m/s (75.8 mph) respectively, the EDR data recorded a longitudinal velocity change of 25.57 m/s (57.2 mph) with a duration of 0.100 seconds for the Tesla, and 27.18 m/s (60.8 mph) and 0.190 seconds for the Toyota. Both the Tesla and Toyota collisions were frontal, with some offset, as evident from post-crash photographs. Both vehicles rotated off of the attenuator and retained some velocity. Maximum lateral velocity changes measured by the EDRs at the B-pillar were 1.07 m/s (2.4 mph) and 2.55 m/s (5.7 mph) for the Tesla and Toyota respectively.

Peak Accelerations and Impact Energy

The ideal triangular crash pulse results in peak accelerations of: 52.2 G (Tesla), 14.6 G (Toyota), 20.2 (Dodge), and 18.4 (Chevrolet). The peak acceleration for the Tesla is more than double any of the other vehicles due to the hard impact to the non-functional attenuator, as evident in the short duration recorded by the EDR. The impact energies are: 799.8 kJ (Tesla), 510.4 kJ (Toyota), 836.1 kJ (Dodge), and 549.8 kJ (Chevrolet). The Tesla and Dodge were significantly heavier than the Toyota and Chevrolet, yielding correspondingly higher impact energies. Due to similar impact energy, attenuator displacements are comparative between the Tesla and Dodge, and between the Toyota and Chevrolet. The Dodge had an attenuator displacement of 5.2 m, which is about 160.8 kJ of energy absorbed per meter of displacement. Using this rate of energy absorption, the Tesla would have benefited from about 5.0 m of displacement. The Chevrolet had 4.8 m of displacement for a rate of about 114.4 kJ per meter. The Toyota likely displaced the attenuator 4.5 m.

DISCUSSION

The purpose of a crash attenuator is to decelerate the impacting vehicle gradually, reducing crash forces at the occupant compartment. The essentially rigid attenuator struck by the Tesla resulted in a very short impact duration and high forces. While the Tesla impact energy was 1.6 times larger than the Toyota, its estimated peak accelerations were 3.6 times higher. The similar impact energy and estimated attenuator displacement for the Tesla to the Dodge indicate that the crash forces would have been similar, had it struck a functional attenuator. Peak accelerations would have been about half of what occurred with the non-functional attenuator. Given that the Toyota driver suffered a tiny intimal aorta tear, the Tesla collision, with roughly triple the impact forces to the passenger compartment, is reasonable to be considered lethal. Reducing that severity with a functional crash attenuator could have saved the Tesla driver, who suffered blunt trauma to the chest and pelvis, and cardiac arrest. This case illustrates the importance of proper maintenance and repair of safety critical traffic safety devices.

REFERENCES

NTSB Accident Report, Collision Between a Sport Utility Vehicle Operating With Partial Driving Automation and a Crash Attenuator Mountain View, California, March 23, 2018, NTSB/HAR-20/01, PB2020-100112, Washington DC.

NTSB Safety Recommendation Report, Addressing Systemic Problems Related to the Timely Repair of Traffic Safety Hardware in California, NTSB/HSR-19/01, August 12, 2019. Available at: https://dms.ntsb.gov/pubdms/search/. Accessed April 12, 2020.

NTSB Docket Item: Crash Attenuator MASH Eligibility and Crash Test Data, Mountain View California, HWY18FH011, Available at: https://dms.ntsb.gov/pubdms/search/. Accessed April 12, 2020.
NTSB Docket Item: Collision with Crash Attenuator – March 12, 2018 Factual Report, Mountain View CA, HWY18FH011, Available at: https://dms.ntsb.gov/pubdms/search/. Accessed April 12, 2020.
NTSB Docket Item: Collision with Crash Attenuator – November 15, 2015 Factual Report, Mountain View CA, HWY18FH011, Available at: https://dms.ntsb.gov/pubdms/search/. Accessed April 12, 2020.

TABLE

Vehicle	Vehicle Mass	Longitudinal Velocity Change	Attenuator Stroke	Peak Accel.	Pulse Duration	Impact Energy
March 28, 2018 crash 2017 Tesla	2,441 kg	25.57 m/s (57.2 mph)	0.0 m	52.2 G	0.100 s	799.8 kJ
March 12, 2018 crash 2010 Toyota Prius	1,380 kg	27.18 m/s (60.8 mph)	unknown	14.6 G	0.190 s	510.4 kJ
KARCO Engineering Test P35022-01 2009 Dodge Ram 1500 pickup	2,270 kg	27.14 m/s (60.7 mph)	5.2 m	20.2 G	0.288 s	835 kJ
KARCO Engineering Test P36142-01 2010 Chevrolet Malibu	1,497 kg	27.09 m/s (60.6 mph)	4.8 m	18.4 G	0.300 s	549 kJ

Friday, October 16th, 2020, 10:55 AM - 11:05 AM EST

Sensitivity of Scale Factor Choice on Injury Response for Equal-Stress Equal-Velocity Scaling

Author: Carolyn Roberts, cwr2tn@virginia.edu
Co-Authors: Jason Forman, jlf3m@virginia.edu, Jason Kerrigan, jrk3z@virginia.edu, Bengt Pipkorn, bengt.pipkorn@autoliv.com

ABSTRACT

Objective: This study aims to evaluate the assumption of geometric similitude inherent to equal-stress equal-velocity scaling by determining if scale factors created with different anthropometry metrics result in different scaled injury tolerance predictions. This assumption will be evaluated when equal-stress equal-velocity scaling is employed across dissimilar (e.g. 50th male to small female) and similar (e.g. small female to a reference small female anthropometry) anthropometries.
Methods: Three average male and three small female lower extremity specimens that were tested in ankle inversion/eversion were selected for scaling analysis. Three additional female specimens were selected as a reference dataset, such that the accuracy of the scaled data could be compared to an independent measured dataset. The failure moments, total height and total weight for these donors were determined from literature. Additional anthropometry metrics (leg length, calcaneus height, and bimalleolar width) were taken from each of their respective CT scans. Scale factors

were calculated from these previously determined anthropometric metrics for the six donors selected for scaling analysis by targeting the averaged anthropometry metrics of the reference small female dataset. Equal-stress equal-velocity scaling was applied to the failure moments from literature using different scale factors. The mean predicted failure tolerance and standard deviation for scaled data using different scale factors were compared to one another and to the mean failure tolerance from the reference (unscaled) small female dataset.
Results: When using average male data to predict ankle failure moment for a small female anthropometry, scaled moments were statistically significantly different from measured small female failure moment. Furthermore, scaled failure moments predicted using scale factors based on different anthropometry metrics were found to be significantly different from one another. Conversely, predicted mean failure moment using scaled female data of a similar size to the reference data was not significantly different from measured female failure moment, and the predicted failure moments were not significantly affected by choice of scale factor.
Conclusions: This study shows that an injury metric predicted with equal-stress equal-velocity scaling is sensitive to choice of scale factor when employing scaling across occupants of dissimilar size and sex. This conclusion suggests error can be introduced into scaled response due to choice of anthropometry metric used to create a scale factor, and therefore, anthropometry metrics used to create scale factors should be justified mechanistically and shown to apply across size and sex before being employed.

INTRODUCTION

Females have been shown to have increased odds of injury and fatality in automobile crashes (Kahane et al, 2013; Forman et al, 2019). Traditionally, female injury tolerance and biomechanical response to impact loading has most frequently been predicted by leveraging measured male cadaveric data and equal-stress equal-velocity scaling, rather than directly measuring female cadaveric response and injury tolerance (Eppinger et al, 1984). Most biofidelity corridors, injury risk functions (IRF), and injury assessment reference values (IARVs) for currently-used female injury prediction tools have been created by applying different combinations of anthropometric scale factors between males and females (Eppinger, 1998; Mertz et al, 2003). Some of these scaling techniques have been related to gross size (e.g. occupant total height and weight) while others take into account local geometry-related metrics (e.g. neck circumference) (Mertz et al, 1997; Davis et al, 2016; Lee et al, 2017). The choice of anthropometry metrics used to create scale factors have not always been justified mechanistically, and an analysis of the sensitivity of scale factor choice has only been performed once for mass-based scale factors within male data, and has never been performed for female data or scaling applied across the sexes (Davis and Gayzik, 2016). As a result, the use of equal-stress equal-velocity scaling for predicting female injury risk may not capture some facets of sexual dimorphism that have an effect on injury risk (Kahane et al, 2013; Forman et al, 2019).

Fundamentally, equal-stress equal-velocity scaling assumes geometric similitude, which, if true, leads to the conclusion that a scaled response should not be highly sensitive to choice of anthropometric variable used to create the scale factor. However, the sensitivity of scaled response to variations in the anthropometric variables used to create scale factors when scaling male data to predict female response (or normalizing male or female data to an idealized size), have not been well-evaluated. Therefore, the goal of this study is to evaluate the assumption of geometric similitude inherent to equal-stress equal-velocity scaling by determining if scale

factors created with different anthropometry metrics result in different injury tolerance predictions. This assumption will be evaluated when equal-stress equal-velocity scaling is employed across dissimilar (e.g. 50^{th} male to small female) and similar (e.g. small female to a single small female anthropometry) anthropometries.

METHODS

Lower extremity computed tomography (CT) scans were obtained from three mid-size male and six small (height =159.3 ± 5.2 cm; weight = 48.6± 8.1 kg) female cadaveric specimens that were tested in dynamic ankle eversion (Funk et al, 2002; Roberts et al, 2018). Anthropometric metrics (total donor height and weight, leg length, calcaneus height, and bimalleolar width) hypothesized to possibly contribute to the response of the ankle were determined from literature or the subject-specific CT scans (Table A1). The data (both CT measurements and measured failure moment) from the three mid-size male donors and a randomly selected three of the six small female donors were used in a scaling analysis. The failure moment data from the remaining three female donors was used as a baseline failure moment dataset to determine the accuracy of the scaled failure moments. The anthropometry measures of these three small female donors were averaged and used as the target anthropometry when scaling was applied. This allowed this baseline small female failure moment dataset to act as a reference dataset to evaluate the accuracy and consistency of scaled response when scaling with different scale factors. After anthropometry measurements were determined from the subject specific CT scans (Table A1) scale factors were determined. These scale factors were used to apply equal-stress equal-velocity scaling to the three male and three female failure moments selected for scaling analysis. The mean scaled failure tolerance and variance of the scaled male and female failure tolerance datasets were compared to measured failure moment from the reference female dataset via paired t-tests. Furthermore, the scaled failure moments predicted using different scale factors were compared using paired t-tests within the scaled male and female datasets to determine if scale factors formed with different anthropometry metrics resulted in significantly different failure moment predictions. This analysis was used to determine if choice of scale factor could result in statistically significant differences in failure moment predicted with equal-stress equal-velocity scaling.

RESULTS

Table 1 shows the values for the predicted mean failure moment and standard deviation when employing scaling to an average male dataset and a small female dataset to predict the failure moment of a reference small female anthropometry using different scale factors. The relative variance in predicted average failure moment across different scale factors is greater within the scaled male dataset (average predicted failure moment: 112.1 +/- 22.0 Nm, coefficient of variation: 20%) than within the scaled female dataset (average predicted failure moment: 69.8 +/- 1.5 Nm, coefficient of variation: 2.1%). Furthermore, the predicted mean failure moment was significantly different ($p \leq 0.05$, paired t-test) for different choices of anthropometry metric used to create scale factors with average male data. This trend did not persist when scaling the small female failure moment data to the reference (small) female anthropometry (i.e. normalizing within the same sex to a similar anthropometry), as different scale factors did not result in statistically significantly different predicted failure moments, and the standard deviation in failure moment was of similar magnitude to the measured small female failure moment. Figure 1 (and Figures A1 and A2) depicts the variance that can be introduced in scaled response when

using different anthropometric measures in scale factor creation for similar size occupants of the same sex (top) and for dissimilar size occupants of different sex (bottom).

DISCUSSION

While limited in sample size, the scaled moment response was less sensitive to the choice of scale factor when the anthropometry to be scaled and the reference anthropometry were close in size and had the same sex. This suggests that geometric similitude might be a more accurate assumption between individuals when the reference and target anthropometries to be used for scaling are similar size and have the same sex (i.e. measured cadaveric tests with donors close to the 50^{th} percentile anthropometry being scaled to the idealized 50^{th} percentile anthropometry). However, it should be noted that while the scaled response is not sensitive to choice of scale factor when the measured and reference geometries are close to one another, it does not necessarily mean that the scaled response is accurate, as scaling has been shown previously to both under- and over-predict measured injury tolerance values for certain loading conditions (Roberts et al, 2018). Furthermore, these results suggest scaling may result in reduced accuracy when applied across different sizes or sexes with scale factors formed from geometric or anthropometric variables that do not directly affect the response that is being scaled. The only way to determine or evaluate if a scale factor is appropriate is to evaluate against measured injury data for donors of different sexes and sizes as a validation. This study highlights the need to collect fundamental cadaveric injury data for a greater range of occupant anthropometries for both sexes to check the assumptions inherent to scaling and quantify their range of applicability. With an improved understanding of fundamental features that correlate to injury risk (and how they vary with sex and gross size), historically-collected cadaveric datasets may be leveraged to more accurately predict the response of a greater proportion of the population. While these results are based on a single body region and loading condition, it seems likely that a sensitivity to choice of scale factor would persist throughout the body; therefore, a mechanistic justification and evaluation of a chosen anthropometry metric used to create a scale factor should always be performed before employing equal-stress equal-velocity scaling.

ACKNOWLEDGEMENTS

This work was supported by Autoliv Research, for which we thank them. The views expressed here are those solely of the authors.

REFERENCES

Davis, M.L. and Scott Gayzik, F.. An objective evaluation of mass scaling techniques utilizing computational human body finite element models. Journal of biomechanical engineering, 138(10). 2016.

Davis, M.L., Koya, B., Schap, J.M. and Gayzik, F.S. Development and full body validation of a 5th percentile female finite element model (No. 2016-22-0015). SAE Technical Paper. 2016.

Eppinger, R.H., Marcus, J.H. and Morgan, R.M. Development of dummy and injury index for NHTSA's thoracic side impact protection research program. SAE transactions. 1984; pp.359-387.

Eppinger, R., Kleinberger, M., Kuppa, S., Saul, R. and Sun, E. Development of improved injury criteria for the assessment of love advanced automotive restraint systems.1998.

Forman, J., Poplin, G.S., Shaw, C.G., McMurry, T.L., Schmidt, K., Ash, J. and Sunnevang, C. Automobile injury trends in the contemporary fleet: Belted occupants in frontal collisions. Traffic injury prevention. 2019; 20(6).
Funk, J.R., Srinivasan, S.C., Crandall, J.R., Khaewpong, N., Eppinger, R.H., Jaffredo, A.S., Potier, P. and Petit, P.Y. The effects of axial preload and dorsiflexion on the tolerance of the ankle/subtalar joint to dynamic inversion and eversion (No. 2002-22-0013). SAE Technical Paper. 2002.
Kahane, C.J. Injury vulnerability and effectiveness of occupant protection technologies for older occupants and women (No. DOT HS 811 766). 2013.
Lee, E, Parent, DP, Craig, MJ, McFadden, J and Moorhouse, K. Biomechanical response requirements manual: THOR 5th percentile female NHTSA advanced frontal dummy. DOT HS 812 370. 2017.
Mertz, H.J., Prasad, P. and Irwin, A.L. Injury risk curves for children and adults in frontal and rear collisions. SAE transactions. 1997; 3563-3580.
Mertz, H.J., Irwin, A.L. and Prasad, P. Biomechanical and scaling bases for frontal and side impact injury assessment reference values (No. 2003-22-0009). SAE Technical Paper. 2003.
Roberts, C., Forman, J. and Kerrigan, J. Injury risk functions for 5th percentile females: ankle inversion and eversion. In Proceedings of the 2018 International IRCOBI Conference. 2018; 702-17.

APPENDICES

Table A2. Anthropometry measures used for creation of scale factors for the three male donors used in the scaling analysis (left), the three small females used in the scaling analysis (middle), and the three small female donors used as the measured reference dataset (right).

	Male Dataset to be Scaled			**Female Dataset to be Scaled**			**Reference Dataset**		
Donor Measurement	**144L (Funk et al 2002**	**116R (Funk et al 2002**	**144R (Funk et al 2002**	**F – 864R (Roberts et al 2018)**	**F – 862L (Roberts et al 2018)**	**F – 866R (Roberts et al 2018)**	**F – 859L (Roberts et al 2018)**	**F – 878R (Roberts et al 2018)**	**F– 856R (Roberts et al 2018)**
Total Height (cm)	**173**	**163**	**173**	**165**	**158**	**155**	**163**	**163**	**152**
Total Weight (kg)	**119**	**92**	**119**	**43.1**	**54.4**	**41.3**	**54**	**59**	**39.9**
Leg Length (mm)	**38.1**	**39.9**	**38.3**	**35.2**	**36.8**	**34.1**	**35.6**	**35.4**	**34.2**
Calcaneus Height (mm)	**60.3**	**58.42**	**59.8**	**53.2**	**54.8**	**58.3**	**56.1**	**51.7**	**54.8**
Bimalleolar Width (mm)	**66.2**	**69.7**	**66.0**	**58.3**	**61.4**	**60.2**	**62.3**	**59.5**	**58.3**

Table A3. Measured and Scaled Failure moments (Nm) for the three different cadaveric datasets (three average males to be scaled, three small females to be scaled, and three small females to act as a reference dataset to evaluate the effectiveness of the scaling and sensitivity of the scaled response).

	Male Dataset to be Scaled			Female Dataset to be Scaled			Reference Dataset		
Failure Moment (Nm)	**M – 144L (Funk et al 2002**	**M – 116R (Funk et al 2002**	**M – 137L (Funk et al 2002**	**F-864R (Roberts et al 2018)**	**F-862L (Roberts et al 2018)**	**F–866R (Roberts et al 2018)**	**F-859L (Roberts et al 2018)**	**F–878R (Roberts et al 2018)**	**F -856R (Roberts et al 2018)**
Measured	**238**	**150**	**99**	**62**	**33**	**107**	**36**	**79**	**68**
Scaled by Total Height	**219**	**146**	**91**	**60**	**33**	**110**	**-**	**-**	**-**
Scaled by Total Weight	**165**	**120**	**69**	**63**	**33**	**118**	**-**	**-**	**-**
Scaled by Leg Length	**152**	**106**	**63**	**63**	**31**	**121**	**-**	**-**	**-**
Scaled by Calcaneus Height	**136**	**98**	**57**	**64**	**31**	**113**	**-**	**-**	**-**
Scaled by Bimalleolar Width	**124**	**84**	**52**	**66**	**30**	**112**	**-**	**-**	**-**

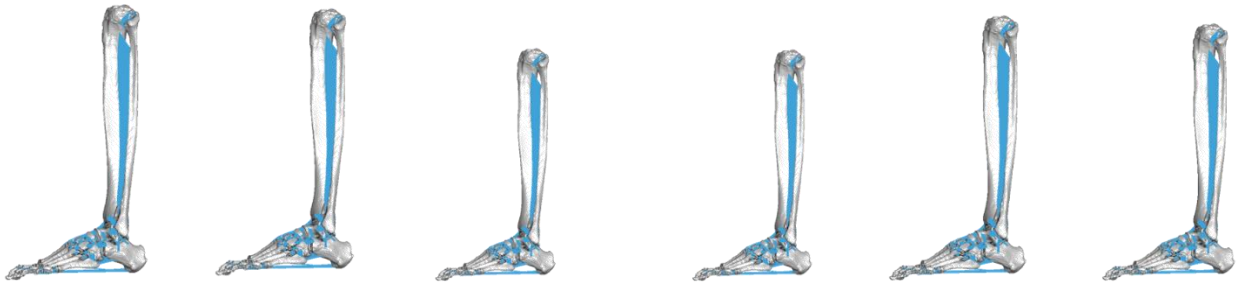

Figure A1. Visual representation of variation in response when using different anthropometric variables from the same male dataset to create different scale factors. In this figure, a male lower extremity geometry was scaled to a small female geometry using different scale factors. The image on the far left represents the unscaled anthropometry. Scale factors used (from left to right) were: total height, total weight, calcaneus height, leg length, and bimalleolar width.

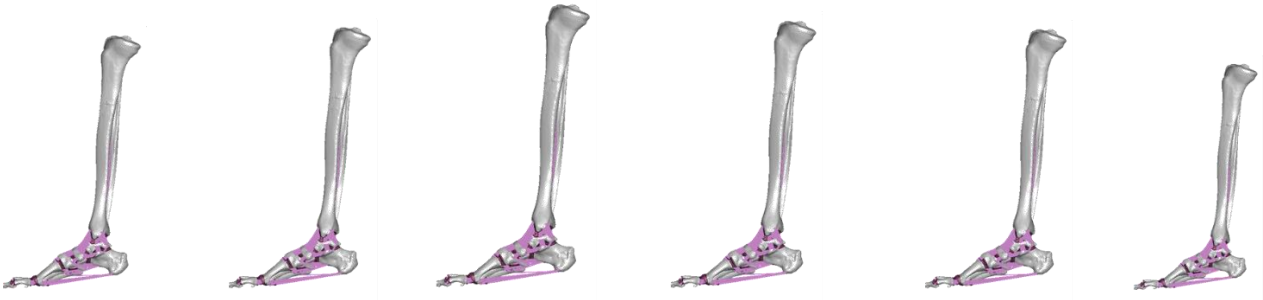

Figure A2. Visual representation of variation in response when using different anthropometric variables from the same female dataset to create different scale factors. In this figure, a small female lower extremity geometry was scaled to a target small female geometry using different scale factors. The image on the far left represents the unscaled anthropometry. Scale factors used (from left to right) were: total height, total weight, calcaneus height, leg length, and bimalleolar width.

TABLES AND FIGURES

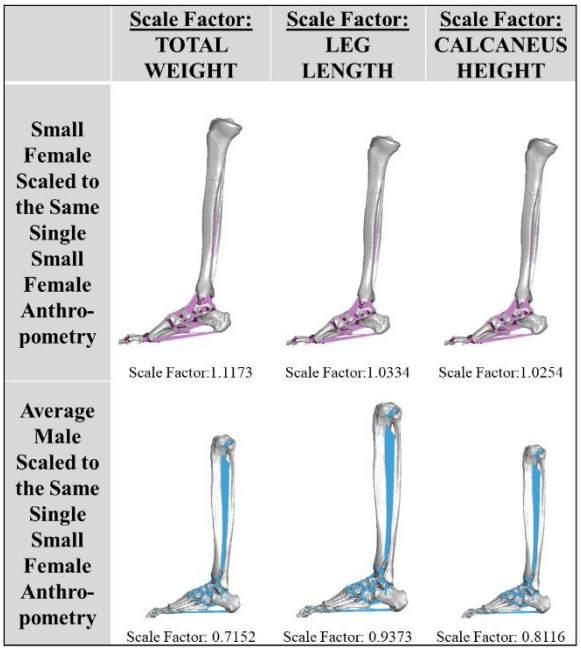

Figure 1. Visual representation of the variation that can be introduced by choice of scale factor when applying equal-stress equal-velocity scaling to between small female and average male anthropometries. The top row shows a single small female anthropometry that has been scaled to a single idealized small female anthropometry using different anthropometric metrics to create scale factors. The bottom row depicts a single average male anthropometry that has been scaled to the same idealized small female anthropometry using scale factors created from three different anthropometric variables.

*Table 1. Average and standard deviation in scaled male and female datasets (columns) when scaled to a target average small female anthropometry when using scale factors based on different anthropometric variables (rows). The measured average failure moment and standard deviation of an additional small female reference dataset is included as a comparison. A pair of * indicates a significant difference from a paired t-test for the average failure moment predicted from the same dataset when using different scale factors, and a † indicates significantly different mean failure moment from the measured reference data*

Average + Stdev Failure Moment (Nm)	**Average male failure moment scaled to small female anthropometry (n=3)**	**Small female failure moment scaled to small female anthropometry (n=3)**
Scale Factor: Total Height	152.1 ± 52.3 *†	67.6 ± 31.7
Scale Factor: Total Weight	117.9 ±39.3 †	71.2 ± 35.2
Scale Factor Leg Length	106.7 ±36.7	71.7 ± 37.3
Scale Factor: Calcaneus Height	97.1 ± 32.5	69.2 ± 33.6
Scale Factor: Bimalleolar Width	86.6 ± 29.4 *	69.5 ± 33.6
Measured Reference Data	**61.0 ± 18.2 (n=3)**	

Friday, October 16th, 2020, 12:45 PM - 12:55 PM EST

Alcohol Use Patterns and Their Association with Sober Driver Vehicle Control in High Fidelity Driving Simulation

Author: Barbara Banz, barbara.banz@yale.edu
Co-Authors: Timothy Brown, timothy-l-brown@uiowa.edu, Deepa Camenga, deepa.camenga@yale.edu, Kaigang Li, kaigang.li@colostate.edu, Federico Vaca, federico.vaca@yale.edu

ABSTRACT

Objective: To examine the relationship between patterns of alcohol use, as determined by the Alcohol Use Disorders Identification Test, and vehicle control measures in high fidelity driving simulation among adult sober drivers.

Methods: Baseline data (BAC=0.00%; N=108) from a larger study aimed at using high-fidelity driving simulation (National Advanced Driving Simulator) to evaluate the feasibility of vehicle-based sensors to identify alcohol impairment were analyzed. Driving simulation scenarios included driving on urban, interstate, and rural roadways. The independent variable was the pattern of alcohol use measured with the Alcohol Use Disorder Identification Test (AUDIT). Dependent variables included one lateral vehicle control measure (i.e., standard deviation of lane position (SDLP)) and one longitudinal vehicle control measure (i.e., average speed relative to the speed limit) in high fidelity driving simulation. Multivariable linear regression was used to examine the associations between patterns of alcohol use and vehicle control measures.

Results: Total AUDIT scores ≥8 was positively associated with SDLP. Increased frequency of drinking was associated with decreased SDLP and increased average speed relative to the speed limit. Increased reports of blackouts and alcohol-related injury were associated with increased average speed relative to the speed limit. Driver performance (SDLP, average speed relative to the speed limit) was related to additional factors such as driver experience, age, marital status, and driving context.

Conclusions: The findings support our hypothesis that the AUDIT score and responses to individual AUDIT questions, among sober drivers, relates to vehicle control measures. Overall, our data highlight two important themes: 1) a need to further integrate alcohol use metrics with high-fidelity driving simulation studies to understand how drinking experience can relate to driver behavior and vehicle control and 2) the opportunity to integrate clinical perspectives with driving simulation research to strengthen clinically oriented alcohol-misuse prevention efforts.

INTRODUCTION

Alcohol-related motor vehicle crashes remain a major public health concern. Recent studies highlight the growing national burden of disease, in both morbidity and mortality, due to alcohol use. In 2018, 29% of all 36,560 crash fatalities were alcohol-related (National Center for Statistics and Analysis 2019). Among those 16 y/o and older, the number of annual alcohol-related deaths doubled between 1999-2017 and the alcohol-related death rate increased by 50% (White et al. 2020). Results from the 2018 National Survey on Drug Use and Health show that 26.5% of adults report binge drinking in the past month with 6.6% reporting heavy alcohol use in the past month (Substance Abuse and Mental Health Services Administration 2019). The US Preventive Services Task Force recommends the screening of adults in clinical settings in order to prevent and reduce alcohol misuse and alcohol-related disease and consequences (O'Connor et al. 2018).

The Alcohol Use Disorders Identification Test (AUDIT), originally developed for screening in a clinical setting, is one of the most widely used and internationally recognized metrics for identifying those with risky/hazardous drinking (Babor et al. 2001). The AUDIT has been successfully used in laboratory studies aimed to understand risky behaviors among non-dependent populations. For example, AUDIT scores have been associated with performance on neuropsychological tests that relate to risky driving behaviors (i.e., impulsivity, inhibition/executive dysfunction, reward sensitivity metrics) (Lyvers et al. 2012), behaviors that put drivers at risk for crash and crash-injury (i.e., making phone calls, sending text messages, not using seat belts), and frequency of drinking and driving (Pharo et al. 2011). The objective of this study was to examine the relationship between patterns of alcohol use, as determined by the AUDIT, vehicle control measures in high fidelity driving simulation among sober adult drivers. An additional goal was to explore how driving performance measures were associated with AUDIT total scores and also responses to individual items or total scores. We hypothesized that total scores and individual AUDIT responses among sober drivers would be related to vehicle control measures during high-fidelity driving simulation.

METHODS

Data for this analysis was from a single study completed at the National Advanced Driving Simulator, University of Iowa (Lee et al. 2010). Study participants were consented and completed a screening prior to scheduling the visit to ensure that they met the study criteria. All participants possessed a U.S. driver's license for at least two years with no restrictions other than vision, drove a minimum of 10,000 miles per year, and did not use any special equipment to drive. Participants in the study were required to be of legal drinking age. For the original study, participants were only included if they were a moderate or heavy drinker as indicated the Quantity Frequency Variability Scale (Cahalan et al. 1969) but had an AUDIT score of ≤ 20. Participants were recruited to fit specific age (21-34 y/o, 38-51 y/o, 55-68 y/o) and gender characteristics. A total of 108 participants were enrolled (36 participants in each of three age groups, 21-34 y/o; 38-51 y/o; 55-68 y/o).

Prior to the simulator drive, participant sobriety was confirmed by an Alco-Sensor IV (BAC=0.00%; Intoximeters, Inc., St. Louis, MO) and a urine sample was provided to screen out those using illegal drugs or drugs that interact with alcohol. The driving scenarios took approximately 35min to complete with urban, interstate, and rural driving conditions. The driving scenario focused on vehicle control. There were no crash-imminent events included. Although the data were collected between 8 a.m. and 1 p.m., all driving scenarios were designed so the participant was driving with nighttime visibility; this was to mimic driving at night since alcohol-involved crashes are most prevalent during nighttime (National Center for Statistics and Analysis 2018). Events extracted from across the single drive for inclusion in the analysis focused on periods of normal driving: urban driving, urban curves, interstate, interstate curves, and rural.

Measures

Alcohol Use Disorder Identification Test (AUDIT): The AUDIT is a 10-item screening survey developed by the World Health Organization to identify alcohol use patterns that are of harmful, hazardous, and dependent. The AUDIT includes questions on drinking behavior (e.g., "How often do you have six or more drinks on one occasion?"), adverse psychological reactions (e.g., "How often during the last year have you been unable to remember what happened the night before because you had been drinking?"), quantity and frequency of consumption (e.g.,

"How often do you have a drink containing alcohol?"), and alcohol-related consequences (e.g., "Have you or someone else been injured as a result of your drinking?") with five responses: 0=never, 1=monthly or less, 2=2-4 times a month, 3=2-3 times a week, and 4=4 or more times a week. For the current analyses we used the sum of the AUDIT score (AUDIT total), domain subscales (Hazardous (sum of items 1-3), Dependence (sum of items 4-6), Harmful Alcohol Use (sum of items 7-10)), and the scores from the individual questions. (Babor et al. 2001). Demographic data were obtained from a survey used to collect data across studies at the NADS (Lee et al. 2010).

Vehicle Control: Vehicle, environment, and driver data were collected at 60-240 Hz and reduced to provide summary data for each driving segment. Dependent measures included measures of lateral (standard deviation of lane position (SDLP)) and longitudinal control (average speed relative to the speed limit).

Analysis

Data were analyzed using SAS v9.4 General Linear Model (GLM) Select function to identify appropriate regression models describing the relationship between patterns of alcohol use and driving performance measured by SDLP and average speed relative to the speed limit. This procedure was selected due to its ability to accommodate continuous dependent measures and combinations of continuous and categorical independent measures. The stepwise selection method was chosen; the Schwarz Bayesian Information Criterion determined model entry/removal. Effect hierarchy was not enforced on model parameters. Available model parameters were individual item responses to AUDIT as well as consumption, dependence, harm and total scores, exceedance of the total score of 8 clinical threshold, age, age group, income marital status, education level, number of children, frequency of driving, miles driven per year, gender, years of driving experience, and age at the start of driving. Although there were instances of multilinearity between some of the variables, removing the variables for sub and total scores, audit score thresholds of 16 and 20, age, and age when starting driving did not affect the stepwise models selected. Road type and event (i.e., urban, urban green light, urban curves, interstate straight, interstate curves, and dark rural road) were included to account for differences in driving environment during the drive.

RESULTS

Elements of the AUDIT were significantly associated with both SDLP and average speed relative to the speed limit as presented in Table 4. SDLP increased by 2.1 cm if the total AUDIT score was greater than or equal to 8 but decreased by 1.0 cm for each step increase on the frequency of drinking. SDLP also increased by 0.01 cm for every year of driving experience. The context of the driving (i.e., road type and event) also effected SDLP. Average speed relative to the speed limit was associated with responses to 3 of the 10 AUDIT questions: drinking frequency (Q1), alcohol-related blackouts (Q8), and alcohol-related injury (Q9). For each step increase in frequency of drinking there was a 0.52 m/s (1.1 mph) increase in average speed relative to the speed limit. For each step increase in frequency of being unable to remember what happened the night before because you had been drinking (i.e. alcohol-related blackout), there was a 0.53 m/s (1.2 mph) increase in average speed relative to the speed limit. For each step increase in frequency of alcohol-related self-injury or injury of another person due to the participant's drinking, there was a 0.58 m/s (1.3 mph) increase in average speed relative to the speed limit. Average speed relative to the speed limit also increased 0.001 m/s (0.001 mph) for

every year of driving experience. Age group was associated with the average speed relative to the speed limit with 38-51 y/o and 55-68 y/o adults driving slower than the 21-34 y/o group (0.67 m/s [1.5 mph] and 2.28 m/s [5.1 mph], respectively). Marital status, income and driving context were also associated with average speed relative to the speed limit.

DISCUSSION

The significant relationship between the widely used AUDIT and simulated driving performance suggests that driving behavior and vehicle control are important factors for clinicians to consider when they screen patients for alcohol use disorder (American Psychological Association 2013). While an alcohol-use survey, like the AUDIT, is generally used to identify ongoing negative consequences of alcohol misuse (i.e., medical and/or social), our findings suggest that the total AUDIT score and even specific AUDIT questions may provide important information about driving behavior among adult sober drivers with a history of drinking. This can serve as a cue to action and guide the clinician-patient conversation about driving habits in the context of their patterns of alcohol use.

We found that total AUDIT scores ≥ 8 were associated with increased SDLP, of approximately 2.1 cm while driving sober, which is approaching the threshold of 2.5 cm often used for identifying clinically significant alcohol impairment (Jongen et al. 2017). Individual AUDIT question responses were also related to vehicle control. Unexpectedly, we found that an increased frequency of drinking was related to reduced SDLP. However, prior research has highlighted important intricacies in studying the relationships between drinking, neurocognitive functioning, and performance (Squeglia et al. 2014). Additionally, individual AUDIT questions on frequency of drinking, alcohol-related blackouts, and either self or harm to others were associated with faster driving. In recent years, alcohol research has highlighted the unique ability for alcohol-related consequences (i.e., blackouts, “harm of others”) to serve as indicators of alcohol misuse and of additional detrimental behaviors, and have become a focus of prevention/intervention efforts aimed at behavioral changes among high-risk drinkers (Vaca et al. 2020; Beynon et al. 2019; Wetherill et al. 2016; Wilhite et al. 2015). Together, our data support the need to evaluate patterns of drinking (e.g., frequency, quantity) as well as alcohol-related consequences in the context of sober driving behaviors and vehicle control.

We recognize this study has limitations. Alcohol use was only measured through the AUDIT. Although the AUDIT is a proven tool for identifying at-risk drinking behaviors in the clinical setting and for drawing empirical comparisons in the laboratory setting, it lacks granularity and specificity in measurement of drinking variables (e.g., binge drinking, age of drinking onset, recency of drinking) which are related to behavioral and performance deficits outside of the driving environment. The original study was designed to develop an algorithm for detecting alcohol impairment behind the wheel, infrequent drinkers and individuals that had an AUDIT score of ≥ 20 were excluded from the original parent study design. As such, we cannot draw conclusions about infrequent or more severe drinking groups. Additionally, not all measures reach practical significance (e.g., the increase of 0.001 mph in driving speed per year of life). However, these data provide evidence for changes over years of which should be further studied for more robust relationships. Finally, the current study was not designed to study additional individual difference variables, such as risk taking or impulsivity, which may relate to drinking and/or driving behaviors. However, these variables are more difficult to evaluate in a clinical setting, unlike the AUDIT which is already extensively used throughout the world and in a multitude of clinical settings. Therefore, when there is concern for patterns of risky drinking, the

healthcare provider/physician can provide additional information on how drinking behaviors relate to driving behaviors which is highly relevant not only to individual injury prevention and health promotion but also to the public's health.

In summary, the current data provides evidence that the drinking patterns among adults with a current BAC of 0.00% are related to differences in driving performance that could translate to unsafe on-road driving behaviors even while sober. Since drinking is a prevalent behavior throughout most of the lifespan, it is important to explore and understand the extent to which screening tools, like the AUDIT, can inform and direct prevention efforts focused on the relationships between drinking patterns and sober driving performance. Our study provides a novel and critical view on the importance of bridging clinical perspectives and high-fidelity driving simulation research in order to inform clinical and injury prevention/intervention efforts.

ACKNOWLEDGEMENTS

The National Highway Traffic Safety Administration funded the collection of the data under contract number: DTNH22-06-D-00043.

REFERENCES

National Center for Statistics and Analysis. 2018 fatal motor vehicle crashes: overview. Washington, DC: National Highway Traffic Safety Administration;2019. Traffic Safety Facts Research Note. Report No. DOT HS 812 826.

White AM, Castle IJP, Hingson RW, Powell PA. Using Death Certificates to Explore Changes in Alcohol-Related Mortality in the United States, 1999 to 2017. Alcoholism: Clinical and Experimental Research. 2020.

Substance Abuse and Mental Health Services Administration. Results from the 2018 National Survey on Drug Use and Health: Detailed tables. Rockville, MD: Center for Behavioral Health Statistics and Quality, Substance Abuse and Mental Health Services Administration;2019.

O'Connor EA, Perdue LA, Senger CA, et al. Screening and behavioral counseling interventions to reduce unhealthy alcohol use in adolescents and adults: updated evidence report and systematic review for the US Preventive Services Task Force. JAMA. 2018;320(18):1910-1928.

National Center for Statistics and Analysis. 2017 Alcohol-impaired driving. Washington, DC: National Highway Traffic Safety Administration;2018. Traffic Safety Facts Research Note. Report No. DOT HS 812 630.

Babor TF, de la Fuente JR, Saunders J, Grant M. The Alcohol Use Disorders Identification Test: Guidelines for use in primary care. 2001.

Lyvers M, Duff H, Basch V, Edwards MS. Rash impulsiveness and reward sensitivity in relation to risky drinking by university students: Potential roles of frontal systems. Addictive behaviors. 2012;37(8):940-946.

Pharo H, Sim C, Graham M, Gross J, Hayne H. Risky business: executive function, personality, and reckless behavior during adolescence and emerging adulthood. Behavioral neuroscience. 2011;125(6):970.

Lee JD, Fiorentino D, Reyes ML, Brown TL, Ahmad O, Fell J, Ward N, Dufour R. Assessing the Feasibility of Vehicle-Based Sensors to Detect Alcohol Impairment. In. Washington, DC: National Highway Traffic Safety Administration; 2010.

Cahalan D, Cisin I, Crossley H. American Drinking Practices. New Brunswick, NJ: Rutgers Center of Alcohol Studies; 1969.

American Psychological Association. Diagnostic and statistical manual of mental disorders (DSM-5®). American Psychiatric Pub; 2013.
Jongen S, Vermeeren A, van der Sluiszen N, Schumacher MB, Theunissen EL, Kuypers KPC, Vuurman EFPM, Ramaekers JG. A pooled analysis of on-the-road highway driving studies in actual traffic measuring standard deviation of lateral position (ie, "weaving") while driving at a blood alcohol concentration of 0.5 g/L. Psychopharmacology. 2017;234(5):837-844.
Squeglia LM, Jacobus J, Tapert SF. The effect of alcohol use on human adolescent brain structures and systems. In: Handbook of clinical neurology. Vol 125. Elsevier; 2014:501-510.
Vaca FE, Li K, Luk JW, Hingson RW, Haynie DL, Simons-Morton BG. Longitudinal associations of 12th-grade binge drinking with risky driving and high-risk drinking. Pediatrics. 2020;145(2). pii: e20184095. doi: 10.1542/peds.2018-4095. Epub 2020 Jan 6.
Beynon C, Bayliss D, Mason J, Sweeney K, Perkins C, Henn C. Alcohol-related harm to others in England: a cross-sectional analysis of national survey data. BMJ open. 2019;9(5).
Wetherill RR, Fromme K. Alcohol-induced blackouts: A review of recent clinical research with practical implications and recommendations for future studies. Alcoholism: clinical and experimental research. 2016;40(5):922-935.
Wilhite ER, Fromme K. Alcohol-induced blackouts and other negative outcomes during the transition out of college. Journal of studies on alcohol and drugs. 2015;76(4):516-524.

TABLES AND FIGURES

Table 4. General Linear Model (GLM) Select results of effects on vehicle control measures.

Parameter	DF	Estimate (*b*)	*t*	Standard Error	*p*-value
Standard Deviation of Lateral Position					
Intercept	1	31.373	23.21	1.352	<.0001
AUDIT Q1 - How Often…	1	-1.045	-2.94	0.355	.0034
AUDIT Total Score ≥8	1	2.139	4.11	0.521	<.0001
Years of Driving Experience	1	0.005	5.98	0.001	<.0001
Event: Urban	1	-3.642	-4.25	0.857	<.0001
Event: Urban Green Light	1	-9.678	-11.29	0.857	<.0001
Event: Urban Curves	0				
Event: Interstate Straight	1	18.395	21.45	0.857	<.0001
Event: Interstate Curves	1	17.535	20.45	0.857	<.0001
Event: Dark Rural Road	1	5.330	6.22	0.857	<.0001
Model df	8				
Error df	543				
Model F-value			227.61		
Mean Speed Relative to Speed Limit					
Intercept	1	1.144	1.62	0.707	0.1061
AUDIT Q1 - How Often…	1	0.514	5.34	0.096	<.0001
AUDIT Q8 - Unable to Remember…	1	0.529	4.15	0.127	<.0001
AUDIT Q9 – Injured…	1	0.580	3.37	0.172	.0008
Years of Driving Experience	1	0.001	2.55	0.0003	.0011
Age: 21-34	0				
Age: 38-51	1	-0.671	-3.74	0.180	.0002
Age: 55-68	1	-2.278	-11.49	0.198	<.0001
Marital Status: Single	1	-1.27	-1.99	0.639	.0469
Marital Status: Married	1	-1.870	-3.08	0.607	.0022
Marital Status: Domestic Partner	1	-1.751	-2.57	0.681	.0104
Marital Status: Separated or Divorced	1	-0.392	-0.61	0.647	.5453
Marital Status: Widowed	0				
Income: Missing	1	-1.148	-2.39	0.480	.0170
Income: $0-$24,999	1	-1.946	-6.47	0.301	<.0001
Income: $25,000 – $29,999	1	-2.175	-4.15	0.524	<.0001
Income: $30,000 - $34,999	1	-1.330	-3.78	0.352	.0002
Income: $35,000 – $39,999	1	-3.707	-9.73	0.381	<.0001

Income: $40,000 - $49,999	1	-0.884	-2.23	0.397	.0265
Income: $50,000 - $59,999	1	-0.348	-1.32	0.264	.1883
Income: $60,000 - $69,999	1	-0.287	-1.23	0.316	.2206
Income: $70,000 - $79,999	1	-1.205	-4.80	0.251	<.0001
Income: $80,000 - $89,999	0				
Income: $90,000 - $99,999	1	-1.012	-3.33	0.304	.0009
Income: $100,000 +	1	-1.013	-4.54	0.223	<.0001
Event: Urban	1	1.682	8.20	0.205	<.0001
Event: Urban Green Light	1	1.432	6.98	0.205	<.0001
Event: Urban Curves	0				
Event: Interstate Straight	1	-2.576	-12.55	0.205	<.0001
Event: Interstate Curves	1	-1.141	-5.56	0.205	<.0001
Event: Dark Rural Road	1	-1.059	-5.16	0.205	<.0001
Model df	26				
Error df	525				
Model F-value			36.72		